



**HAL**  
open science

# Comprehensive analysis of alternating current electrokinetics induced motion of colloidal particles in a three-dimensional microfluidic chip

Thibault Honegger, David Peyrade

► **To cite this version:**

Thibault Honegger, David Peyrade. Comprehensive analysis of alternating current electrokinetics induced motion of colloidal particles in a three-dimensional microfluidic chip. *Journal of Applied Physics*, 2013, 113 (19), pp.194702. 10.1063/1.4804304 . hal-00937008

**HAL Id: hal-00937008**

**<https://hal.science/hal-00937008v1>**

Submitted on 16 Dec 2022

**HAL** is a multi-disciplinary open access archive for the deposit and dissemination of scientific research documents, whether they are published or not. The documents may come from teaching and research institutions in France or abroad, or from public or private research centers.

L'archive ouverte pluridisciplinaire **HAL**, est destinée au dépôt et à la diffusion de documents scientifiques de niveau recherche, publiés ou non, émanant des établissements d'enseignement et de recherche français ou étrangers, des laboratoires publics ou privés.

# Comprehensive analysis of alternating current electrokinetics induced motion of colloidal particles in a three-dimensional microfluidic chip

Thibault Honegger and David Peyrade<sup>a)</sup>

LTM--CNRS UJF INP c/o CEA--LETI--MINATEC, 17 avenue des Martyrs, 38054 Grenoble cedex 9, France

(Received 30 October 2012; accepted 22 April 2013; published online 20 May 2013)

AC electrokinetics is becoming a strategic tool for lab-on-a-chip systems due to its versatility and its high level of integration. The ability to foresee the behaviour of fluids and particles under non-uniform AC electric fields is important to allow new generations of devices. Though most of studies predicted motion of particles in co-planar electrodes configurations, we explore a pure 3-D AC electrokinetic effect that can open the way to enhance contact-less handling throughout the microchannel. By fabricating 3D microfluidic chips with a bi-layer electrodes configuration where electrodes are patterned on both sides of the microfluidic channel, we present a detailed study of the AC electrokinetic regimes that govern particles motion suspended in different host media subjected to a non-uniform AC electric field that spreads through the cross-section of the microchannel. We simulate and observe the motion of 1, 5, and 10  $\mu\text{m}$  polystyrene particles relative to the electrodes and provide an insight on the competition between electro-hydrodynamical forces and dielectrophoresis. We demonstrate that using relevant electrode designs combined with the appropriate applied AC potential, particles can be handled in 3-D in the micro-channel at a single or a collective level in several medium conductivities. Both numerical simulations and experimental results provide a useful basis for future biological applications. © 2013 AIP Publishing LLC. [<http://dx.doi.org/10.1063/1.4804304>]

## I. INTRODUCTION

Since microfluidics has opened access to high strength electric fields ( $>10^5$  V/m) in confined environments, electrokinetics has been widely used to manipulate beads or cells. Electrokinetic phenomena have a great potential for biological applications, especially in cellomics. Several devices have been presented<sup>1</sup> to focus,<sup>2–6</sup> separate,<sup>7–9</sup> organize,<sup>5,10–13</sup> or handle<sup>14–16</sup> polarizable micro- to nano-objects when applying potentials within the fluid.

Since DC voltages can produce electrolysis of water, the application of AC potentials is preferred. Those potentials create a force named Dielectrophoresis (DEP), a term introduced by Pohl,<sup>17</sup> that occurs in polarizable objects induced by a non-uniform electric field. AC potentials also cause motion of the fluid by electrohydrodynamical (EHD) forces, namely, AC electro-osmosis (ACEO)<sup>18</sup> and the electrothermal effect (ETE).<sup>19</sup> Those phenomena drive bulk fluid motion and drag particles along. When submitted to both EHD and DEP forces, movement of micro- and nano-particle in AC electrokinetics devices can be difficult to analyse and predict. Several studies have presented the competition between DEP, ACEO, and ETE forces in 2-D configurations, i.e. coplanar electrodes geometries.<sup>19–24</sup> Such configuration of electrodes has been widely used to manipulate particles in closed PDMS microchannels. However, by essence, coplanar electrodes geometries have a close proximity effect on objects and flow can release trapped particles by dragging them.<sup>25,26</sup> This limitation of co-planar electrodes prevents them from being used in fully integrated lab-on-chip systems for high throughputs

applications. We believe that 3-D configuration electrodes can overcome those limitations and open the way to new devices and applications.

The ability to fabricate 3-D electrodes,<sup>27–29</sup> i.e., electrodes that are designed on the top and the lower parts of the confined colloidal solution, has led to devices capable of trapping particles while sustaining flows. Such devices could provide tools for precise 3-D handling of particles but also to trap cells under continuous media replacement, such as in perfusion devices. Very low volumes of liquid are required to fill a microchannel (e.g., 200 nl of liquid for a typical channel size of height 20, width 500, and length 20 000  $\mu\text{m}$ ) and swapping liquids while trapping cells could provide tools for high throughput drug discovery. However, biological samples are generally suspended in buffer solutions that present high electrical conductivities (Phosphate buffer solution (PBS)  $1\times$  has a conductivity of 1.42 S/m and Dulbecco's Modified Eagle Medium (DMEM) of 1.38 S/m). The conductivity of the medium plays a significant role in the relative strengths of EHD and DEP forces and studies have more commonly presented the impact of such high conductivities on the AC electrokinetics forces in 2-D<sup>20–22,24,30</sup> than in 3-D electrodes configurations.<sup>27,31–33</sup>

This work presents a systematic study of the motion of micrometer range polystyrene (PS) particles under 3-D electrodes configurations. Particles have been suspended into 3 buffer solutions with varying conductivities: DI water, salted water, and DMEM. We investigate the motion of particles within several 3-D configurations of electrodes: vertical bars, donut trap, and perpendicular bars. We have chosen those designs to be most of interest for future applications for separation, trap, or manipulation of cells. We first introduce the

<sup>a)</sup>Electronic mail: david.peyrade@cea.fr

theoretical background of EHD and DEP forces. Then, we present a detailed simulation of the AC electrokinetic phenomena and give a frequency-voltage mapping for particle trapping. Finally, we investigate the validity of the theory with experimental results. Therefore, we demonstrate the motion and manipulation of particles in a 3-D configuration of electrodes, and confirm the ability of such devices to position particles not only in close proximity to the electrodes but also in the center of the microchannel.

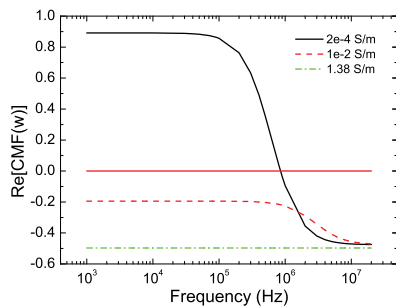
## II. THEORY

### A. Dielectrophoresis

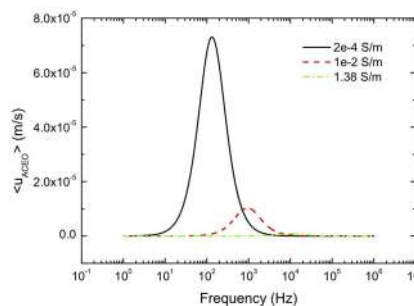
DEP is a force that appears in a polarizable particle (diameter  $a$ , permittivity  $\epsilon_p$ , conductivity  $\sigma_p$ ) suspended in a polarizable medium (permittivity  $\epsilon_m$ , conductivity  $\sigma_m$ ) when immersed in a non-uniform electric field ( $\vec{E}$ ). For a spherical particle, this force can be written as Eq. (1). The factor  $Re[CMF(\omega)]$  is known as the Clausius-Mossotti factor (CMF) and translates the difference of polarizability of the particles and its suspending medium. As presented in Eq. (2),  $Re[CMF(\omega)]$  depends on the physical characteristics of the particle and of the medium but also on the frequency of the AC electric field. Therefore, when the particle is more polarizable than the medium, the dipole induced by the electric field responds to the gradient of this field which attracts the particle to regions where the electric field gradient is the maximum (typically at the borders of the electrodes). This regime is named positive dielectrophoresis (pDEP). On the contrary, when the particle is less polarizable than the medium, the particle is repelled from high gradient regions. This regime is named negative dielectrophoresis (nDEP). This versatility makes DEP a very unique contact-less force for attracting and repelling polarizable objects only by tuning the AC frequency. Comparatively, switching from repulsion to attraction is not possible with the application of capillary<sup>34</sup> or optical<sup>35</sup> forces in order to control particle trapping

$$\langle F_{DEP} \rangle = \pi \epsilon_m a^3 Re[CMF(\omega)] \nabla |E|^2, \text{ where } |E|^2 = E \cdot E^*, \quad (1)$$

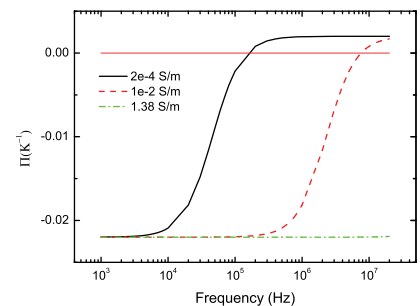
$$Re[CMF(\omega)] = \frac{\tilde{\epsilon}_p - \tilde{\epsilon}_m}{\tilde{\epsilon}_p + 2\tilde{\epsilon}_m}, \quad (2)$$



(a)



(b)



(c)

FIG. 1. (a):  $Re[CMF(\omega)]$  for PS particles suspended in raising medium conductivity. (b):  $\langle u_{ACEO} \rangle$  of ACEO as a function of AC frequency for several conductivities of the fluidic medium when  $E_t = 10^6$  V/m. (c): Evolution of  $\Pi$  factor from ETE as a function of frequency for several conductivities of the medium.

$$\tilde{\epsilon}_{m/p} = \epsilon_{m/p} - i \frac{\sigma_{m/p}}{\omega}, \quad (3)$$

whereas the electrodes geometry defines the spatial variation of the field gradient, the CMF dictates the direction and strength of the DEP force. As reported by previous works,<sup>36–38</sup> the conductivity of a solid homogeneous non-metallic spherical particle (such as a PS sphere) is given by Eq. (4), where  $a$  is the particle radius and  $K_s$  its the surface capacitance. For PS spheres, the bulk conductivity is negligible, so that the effective conductivity of the particle is dominated by the surface conductance (typical values are of the order of 1 nS (Refs. 39 and 40))

$$\sigma_p = \sigma_{bulk} + 2 \frac{K_s}{a}. \quad (4)$$

The CMF of plain, i.e. non surface modified, PS particles are shown in Fig. 1(a). The real part of the CMF for particles varies from positive to negative with a specific crossover frequency at which  $Re[CMF(\omega)] = 0$  (corresponding to a net zero DEP force). As plotted in Fig. 1(a), when varying the conductivity of the medium from DI water ( $\sigma_m = 2.10^{-4}$  S/m) to biological medium (PBS,  $\sigma_m = 1.38$  S/m), plain PS particles tend to have a negative response. This behaviour can vary from one particle-medium pair to another. Moreover, in the case of anisotropic particles<sup>16,41</sup> or cells, the values of  $Re[CMF(\omega)]$  can present 2 crossover frequencies.<sup>40,42</sup> Recent works<sup>39,40</sup> have presented a method to determine experimentally  $Re[CMF(\omega)]$  and to extract the intrinsic physical parameters (surface conductance in a single or multi-shell model) of polarizable particles as soon as they can be tracked individually. The complete determination of  $Re[CMF(\omega)]$  is crucial to manipulate with accuracy polarizable particles by DEP.

However, applying an electric field in a liquid also induces motion of the fluid itself. This motion drags the particles along with the fluid. Such phenomena, known as AC electroosmosis or the electrothermal effect, are discussed below.

### B. AC electro-osmosis

ACEO refers to the flow motion created at the electrodes surfaces when AC signals are applied. The induced surface charges at the electrode/electrolyte interface attract

counter-ions from the solution and repel co-ions from the surface to maintain minimal local charge neutrality. Consequently, an excess of charges is built up near the electrodes surfaces, thus forming an electrical double layer. The counter-ions in this double layer will migrate under the influence of the tangential field and drag the rest of the liquid towards the electrodes. The volumic force will convey particles towards the surface of the electrodes. Most ACEO devices reported so far adopt a co-planar electrodes configuration.<sup>20-22</sup> Recent works<sup>43,44</sup> have presented asymmetric face-to-face pairs of electrodes for particle concentration on one electrode. The fluid motion on the electrode is obtained from the Helmholtz-Smoluchowski velocity given in Eq. (5). The zeta potential is developed in Eq. (6) where  $\sigma_{qd}$  is the diffuse layer charge density of the solid/liquid interface. Since most of microfluidic chips consist of electrodes on glass slides, we use the value of the borosilicate glass measured in DI water ( $\sigma_{qd} = -0.32 \text{ mC} \cdot \text{m}^{-2}$ ) by Micheletto<sup>45</sup> in our simulations. In the case of co-planar electrodes, the potential drop across the double layer is spatially varying, which leads to an induced zeta potential. In our case, bi-layer electrodes induce a uniform electric field on their faces and thus present a constant zeta potential as suggested by previous work<sup>43,44</sup>

$$u_{ACEO} = \frac{\varepsilon_m}{\eta_m} \zeta E_t, \quad (5)$$

$$\zeta = -\frac{\sigma_{qd} \lambda_d}{\varepsilon_m}. \quad (6)$$

The creation of the boundary slip velocity requires both the tangential electric field and the charged ions at the interface. Therefore, there exists an optimal AC frequency at which the product of the electric field and the interface zeta potential reaches a maximum. For a frequency that is lower than the optimal frequency, the capacitance induced by the ions at the electrode/liquid interface is much larger than the bulk liquid and the potential drops within this layer. The electric field that can penetrate through the double layer is small, resulting in a small tangential electric field. This also yields to a small slip velocity. On the contrary, for a frequency that is much higher than the optimal one, the electrode/liquid capacitor is saturated and the potential drop within the double layer induces a small zeta potential, resulting in a small slip velocity. The frequency dependency of face-to-face electrodes can be estimated by introducing a non-dimensional frequency  $\Omega_{ACEO}$

$$\Omega_{ACEO} = \frac{\pi L}{2} \frac{\varepsilon_m}{\lambda_d \sigma_m} \omega, \quad (7)$$

where  $L$  is the distance between the electrode,  $\lambda_d$  is the double-layer thickness,  $\sigma_m$  is the conductivity of the liquid medium, and  $\varepsilon_m$  is the permittivity of the liquid. Finally, the time average velocity of asymmetric face-to-face electrodes can be given by

$$\langle u_{ACEO} \rangle = \frac{\varepsilon_m}{\eta_m} \zeta \frac{\Omega_{ACEO}^2}{(1 + \Omega_{ACEO}^2)^2} E_t. \quad (8)$$

Calculation of the ACEO velocity on the electrodes is presented in Fig. 1(b) with a tangential electric field of  $E_t = 10^6 \text{ V/m}$ .

The velocity of the fluid diminishes when raising the medium conductivity. Since the double layer thickness decreases with the conductivity, the zeta potential falls, and thus the velocity also falls. A shift in frequency can also be spotted and maximum velocities are reached for 200 Hz when  $\sigma_m = 2 \times 10^{-4} \text{ S/m}$ , for 1 kHz when  $\sigma_m = 10^{-2} \text{ S/m}$ , and for 10 kHz when  $\sigma_m = 1.38 \text{ S/m}$ .

### C. Electrothermal effect

When an electric field  $E$  is applied over the fluid (electrical conductivity  $\sigma_m$ ), Joule heating is produced inside the fluid according to the energy balance equation (9),<sup>19</sup> where  $T$  is the temperature and  $k$  is the thermal conductivity of the fluid. If the field is non-uniform, there will be spatial variation in heat generation, which leads to temperature gradient  $\nabla T$  in the fluid. This variation produces spatial gradients in the local permittivity and conductivity, given as  $\alpha$  (10) and  $\beta$  (11), respectively. Furthermore, those gradients generate mobile space charges,  $\rho$ , in the bulk fluid, following  $\rho = \nabla(\varepsilon_m E) = \nabla \varepsilon_m E + \varepsilon_m \nabla E$  and  $d\rho/dt + \nabla(\sigma_m E) = 0$  in AC fields. The time average of the electric force that acts on the fluid through viscosity and leads to fluid transport is given as Eq. (13), where the  $\Pi$  factor plays a significant role in the magnitude and direction of the force as shown in Fig. 1(c). When the left term on Eq. (14) is greater than the right one,  $\Pi$  is positive and the fluid flows from the edge to the center of the electrode. For negative values of  $\Pi$ , the flow pattern is in the opposite direction

$$k \nabla^2 T + \sigma E^2 = 0, \quad (9)$$

$$\alpha = \frac{1}{\varepsilon_m} \frac{\nabla \varepsilon_m}{\nabla T} = -0.4\% \text{K}^{-1}, \quad (10)$$

$$\beta = \frac{1}{\sigma_m} \frac{\nabla \sigma_m}{\nabla T} = 2\% \text{K}^{-1}, \quad (11)$$

$$\tau_m = \varepsilon_m / \sigma_m, \quad (12)$$

$$\begin{aligned} \langle \vec{F}_{ETE} \rangle &= -\frac{1}{2} \left[ \frac{\varepsilon_m \left( \frac{\nabla \sigma_m}{\sigma_m} - \frac{\nabla \varepsilon_m}{\varepsilon_m} \right) \vec{E} \cdot \vec{E}}{1 + (\omega \tau_m)^2} + \frac{1}{2} |\vec{E}|^2 \nabla \varepsilon_m \right] \\ &= \frac{1}{2} \varepsilon_m \nabla T E^2 \Pi(\omega), \end{aligned} \quad (13)$$

$$\Pi(\omega) = \left( \frac{\alpha - \beta}{1 + (\omega \tau_m)^2} - \frac{\alpha}{2} \right). \quad (14)$$

In this work, we do not take under account the possible source of temperature gradient that could rise from the microscope illumination light. This type of excitation is present in a microfluidic system but it has been shown to be much less than the ETE body force.<sup>19</sup>



To conclude this theoretical part, the application of an AC electric field inside the fluid creates two major EHD phenomena, ACEO and ETE, that settle a competition with DEP. Those effects will generate fluid motion and alter the dielectrophoretic manipulation of particles. Whereas ACEO is a dominant force for small frequencies of the AC field (typically below 10 kHz) and decreases in magnitude when raising the conductivity of the medium, ETE will remain constant at all frequencies and strongly increasing with the conductivity of the medium. Moreover, DEP will be dominant for  $10^6$  Hz range frequencies or when the conductivity of the medium is low ( $\sigma_m < 10^{-2}$  S/m). In the conductivity range of biological medium, in the order of 1 S/m, EHD forces are still dominant but there exists a window of operation in which DEP is still active ( $V \lesssim 2V_{p-p}$ ) and where biological sample can be addressed.

### III. MATERIALS AND METHODS

#### A. Microfabricated devices and materials

AC electrokinetics experiments have been conducted on a transparent, multi-level electrodes microfluidic chip.<sup>28,46</sup> The microfluidic chip consists of a photopatternable PDMS (PPS) layer sandwiched between a top and a lower glass slides patterned with etched Indium Tin Oxide (ITO) electrodes. The microchannel is opened on the top and the bottom slides during the photolithography step without any PDMS residual layer (Fig. 2(a)). Its shape is rectangular ( $500 \mu\text{m} \times 20 \mu\text{m}$  cross-section). The ITO electrodes (150 nm layer thickness) are directly in contact within the fluid. Three geometries of electrodes are investigated: parallel bars (Fig. 2(b)), donuts (Fig. 2(c)), and perpendicular bars (Fig. 2(d)). Electrodes are  $10 \mu\text{m}$  wide and the inner diameter of a donut electrode is  $15 \mu\text{m}$ .

Each design offers unique handling properties. All our designs are implanted in 3 microfluidic chips in which the channel height (PPS layer) was chosen to be  $20 \mu\text{m}$ .

- *Parallel bars (PaB)*: Parallel bars are perpendicular to the microchannel (Fig. 2(b)) and can provide a *stop* function that prevents colloidal particles from passing through it. According to the CMF properties of a population of particles, parallel bars can also work as a particle sorter: Applying an AC frequency at which one type of particle presents  $Re[CMF(\omega)] = 0$  whereas another type presents a negative one can prevent the latter to pass through it.<sup>27,47</sup> Our designs consist of 2 bars of  $10 \mu\text{m}$  width through the entire width of the microchannel.
- *Donut trap (DT)*: The donut trap consists of 2 concentric rings (Fig. 2(c)). One of them is grounded whereas the other

one is connected to the AC potential. Such rings, or donut, can create a trap with a nDEP cage. Unlike other designs such as co-planar squared traps,<sup>26</sup> planar ring traps,<sup>48</sup> or octopoles 3-D traps,<sup>49</sup> our 3-D design can sustain liquid flow in all directions. Moreover, this design does not allow any other particle to penetrate the trap. This design consists of several concentric rings on the top and lower slides connected side-by-side. The width of the ring is  $10 \mu\text{m}$  and the diameter of the inner circle of the ring is  $15 \mu\text{m}$ .

- *Perpendicular Bars (PeB)*: Perpendicular bars are two linear electrodes that are perpendicular one to each other (Fig. 2(d)). This design was first presented for Moving DEP (mDEP) that has been shown to manipulate beads or cells.<sup>50</sup> The general idea is to induce motion of particles by moving the electric field via an array of electrodes. The applied potential can induce either positive or negative DEP for a certain amount of time on the bead. A specific sequence will control the bead movement to a targeted location. Few works<sup>50-52</sup> have been done on this 3-D configuration, especially considering the effect of induced fluid motion. Our design consists of an array of vertically aligned  $10 \mu\text{m}$  width electrodes separated by  $10 \mu\text{m}$ . One array is placed on the top slide and another one is aligned perpendicularly to it on the lower slide. Each electrode can be activated independently to an AC potential.

Fluidic connections are ensured by Upchurch Nanoport (N-333) connectors and fluid is pushed into the microchannel by a remotely controlled syringe pump. This pump will push a fixed amount of air that will push the liquid inside the chip. By doing so, the “cap” effect<sup>53</sup> is avoided and particles motion can be easily controlled inside the chip.

#### B. Simulations

Simulations of the forces were performed by a finite element method using COMSOL MULTIPHYSICS (COMSOL). Each design was modelled according to the geometries given in previous paragraph. We have chosen to model the electrodes with no height, i.e., as boundary conditions on the borders of the channel. Since the thickness of the ITO electrodes (170 nm) are small ( $<1\%$ ) compared to the channel height ( $20 \mu\text{m}$ ), they can be modelled as boundary electrostatic potentials without modifying the electric field compared to extruded ones.<sup>54</sup> The final mesh of the system was refined (100 nm) near the borders of the channel.

In order to compute the slip velocity induced by ACEO, the tangent electric field for each design is computed on the borders of the electrodes.

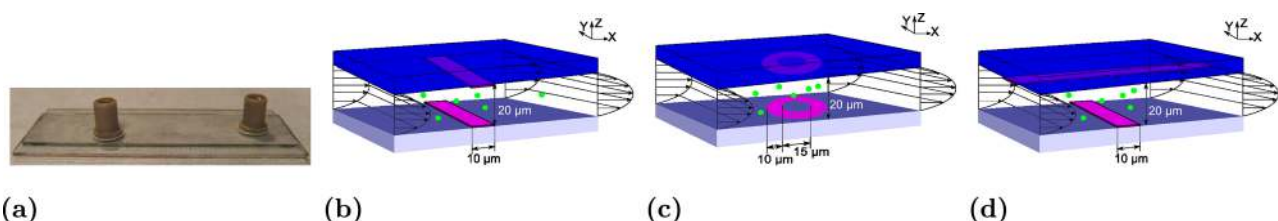


FIG. 2. (a) ITO microfluidic chip. Schematic of designed electrode pairs: (b) Parallel bars trap, (c) donut trap, and (d) perpendicular bars trap. All lower electrodes are grounded and upper electrodes are put to an AC potential. Fluid motion is indicated by black arrows.

Four parameters are varied: conductivity of the buffer  $\sigma_m$ , diameter of the particle  $a$ , applied voltage  $V_{p-p}$ , and frequency  $f$  of the AC signal. For all simulations, a first step consists of computing  $Re[CMF(\omega)]$ ,  $\Pi$  and  $\Omega_{ACEO}$  factors for each set of parameters. 3 models are then applied:

- *Electrostatics*: The spatial distribution of the electric field and the voltage is computed.
- *Thermal diffusion*: The spatial distribution of the temperature and its gradient induced by the electric field are calculated.
- *Incompressible Navier-Stokes flow*: The flow velocity is given by the combination of the volume ETE induced velocity (which acts like a body force on the liquid) and the surface ACEO induced velocity (which acts as a slip velocity on the electrodes).

The assembly of each force is performed in post processing mode. The DEP force  $F_{DEP}$  is computed for a given mesh point with  $\nabla|E|^2$  for each parameters. The global EHD force  $F_{EHD}$  is the sum of the ACEO and ETE velocities that act on the liquid. This velocity is converted as a drag force acting on the particle<sup>19</sup> according to Eq. (15). In our simulations, we consider the particle to be at rest ( $v_p = 0$ ) when the electrokinetic forces first appear. The gravity force  $F_{grav}$  is summed to  $F_{EHD}$  according to Eq. (16). Finally, all forces are summed into  $F_{Tot}$

$$F_{drag} = 6\pi\eta_m a(v_p - v_{fluid}), \quad (15)$$

$$F_{grav} = \frac{4}{3}\pi\left(\frac{a}{2}\right)^3(\rho_p - \rho_m)g. \quad (16)$$

### C. The electro-microfluidic platform

The chip is inserted into a home-made electro-microfluidic platform that creates up to 112 electrical connections via a zero force insertion module<sup>55</sup> (Fig. 3(a)). Each contact is by default grounded and can be connected to an AC voltage via an electronic home-made device. The platform (Fig. 3(a)), based on a modified Leica microscope, is controlled in real-time with a home-made Labview program (National Instrument) for the fluidic module, the electrical module, and for the observation module.

In order to visualize the flow pattern in the X-Z plane, a cleaved microfluidic chip is fabricated according to the same

protocol. The electrode design consists of 2 pairs of electrodes separated by  $15\ \mu\text{m}$  as presented in Fig. 3. The final stack is cleaved on both sides with a diamond tip. A colloidal drop is deposited on the side of the stack and capillary forces drag the solution into the channel. A small glass slide is then placed in front of the stack to avoid meniscus formation which allows monitoring the motions of particles from the side. Particles are illuminated from the top through a  $20\times$  microscope objective and scattered fluorescence is observed from the side through a  $50\times$  long focal distance objective. Electrical connections are activated by clipping the electrodes far from the channel. Top and bottom electrodes are, respectively, put to the AC potential and grounded. Such configuration of electrodes matches either the median X-Z plane of the donut trap or the X-Z plane of a focalisation-funnel design.<sup>3,28,56</sup> A side-view picture of the platform is presented in Fig. 3(b).

### D. Particles and solution preparation

PS particles are purchased from Duke (diameter 1, 5, and  $10\ \mu\text{m}$ ) and resuspended 3 times by a centrifugation-resuspension process in 3 different buffer solutions with increasing conductivities: DI Water ( $\sigma_m = 2 \times 10^{-4}\ \text{S/m}$ ), NaCl saline solution ( $\sigma_m = 10^{-2}\ \text{S/m}$ ), and cell culture medium, Dulbecco's Modified Eagle Medium (DMEM + 10% SVF + 1% ATAM (Hela)) ( $\sigma_m = 1.38\ \text{S/m}$ ). Each solution contained 1% wt. of particles. Buffer solutions were freshly prepared before experiments and conductivities were measured with a mobile conductimeter (COND6 + from Eutech instruments).

### E. Experimental protocol

Before injection in the microfluidic chip, the colloidal solution is vortexed in order to maintain a uniform dispersion. Particles are injected at a mean constant velocity of  $50\ \mu\text{m/s}$  ( $50\ \text{nl/min}$ ) to avoid any sedimentation. As soon as the channel is filled, the pressure maintained by the syringe pump is lowered so that particles motions are only Brownian. AC potentials were then applied on targeted electrodes. A sequence of frequencies, voltages and application durations are programmed. Particles motion movies are then compressed and time-adjusted according to the recording frame-rate (20 fps) so that all movies present the same time frame. Particle tracking velocities are extracted from recorded

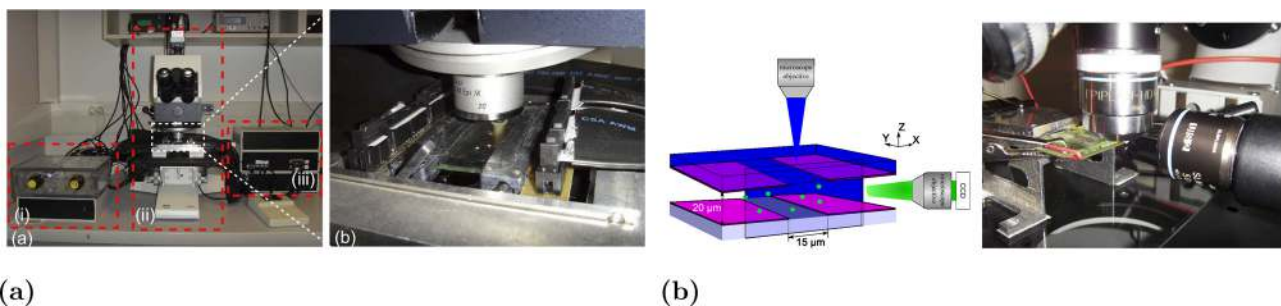


FIG. 3. (a): Home-made electro-microfluidic platform: (i) Fluidic module with a pressure driven flow (flow: 0-1 nl/s with a  $100\ \mu\text{l}$  injection loop); (ii) Holder and observation module (Obj.  $5\times 20\times 50\times$  - Dark-field - Fluorescence); (iii) Electrical re-routing module of the AC potential via microcontrollers and electromagnetic relay via the chip electrical connections. (b) Zoom on the chip holder with alignment of the chip to the electrical connections via the zero force insertion module. (c) Schematic view and side-view picture of the electro-microfluidic platform that allows access to X-Z plane velocities. Particles are illuminated by a microscope objective from the top and scattered fluorescence is recorded from the side.

movies and analyzed with IMAGEJ. Once the sequence is accomplished, the particles are pushed out of the microchannel that is washed 3 times with ethanol before the next experiment. Movies of particles motion are recorded with a LABVIEW program that controls entirely the platform in real-time. When used, particles in the microfluidic channel are counted with an IMAGEJ plugin “Particle tracker.”<sup>57</sup>

## IV. RESULTS AND DISCUSSION

### A. Simulations: Visualisation of the forces

Isosurfaces represent  $\nabla|E|^2$  ( $V^2m^{-1}$ ) and arrows the negative dielectrophoretic force (N). The channel height is  $20\ \mu m$  and the applied potential is  $2\ V_{p-p}$ .

We first visualize  $\nabla|E|^2$  for each electrode design to foresee the direction of the nDEP force, typically the most observed case when the medium conductivity is high. Fig. 4 shows the COMSOL simulation for the designed electrodes in 3-D views. The vertical bars (Fig. 4(a)) present a clear repulsive force from the electrode edges on the top view but also on the side view. The directions of the nDEP forces indicate

that particles will be repelled from the electrodes but also focused in the center of the channel. When injecting liquid, the flow may pass through the electrodes whereas particles may stay in front of them.

For the donut trap design, the nDEP forces create a cage and push the particle to be trapped in the center of the concentric rings but also in the middle of the channel. Moreover, particles could not pass through this trap since nDEP forces act also on the outer edges of the rings. In the same way as for the parallel bars, flow will continue to pass through the electrodes whereas particles will be trapped and their position will be maintained in 3-D. Finally, the perpendicular bars design shows a repulsive force from the bottom electrode that will repel particles from its edges whereas the top electrode will repel them from the entire electrode (gradients are all over the upper electrode).

Based on the models described in Sec. II, we simulate the directions and strengths of the AC electrokinetic forces to understand the experimental observations of the particles motion induced by the competition between EHD and DEP forces.

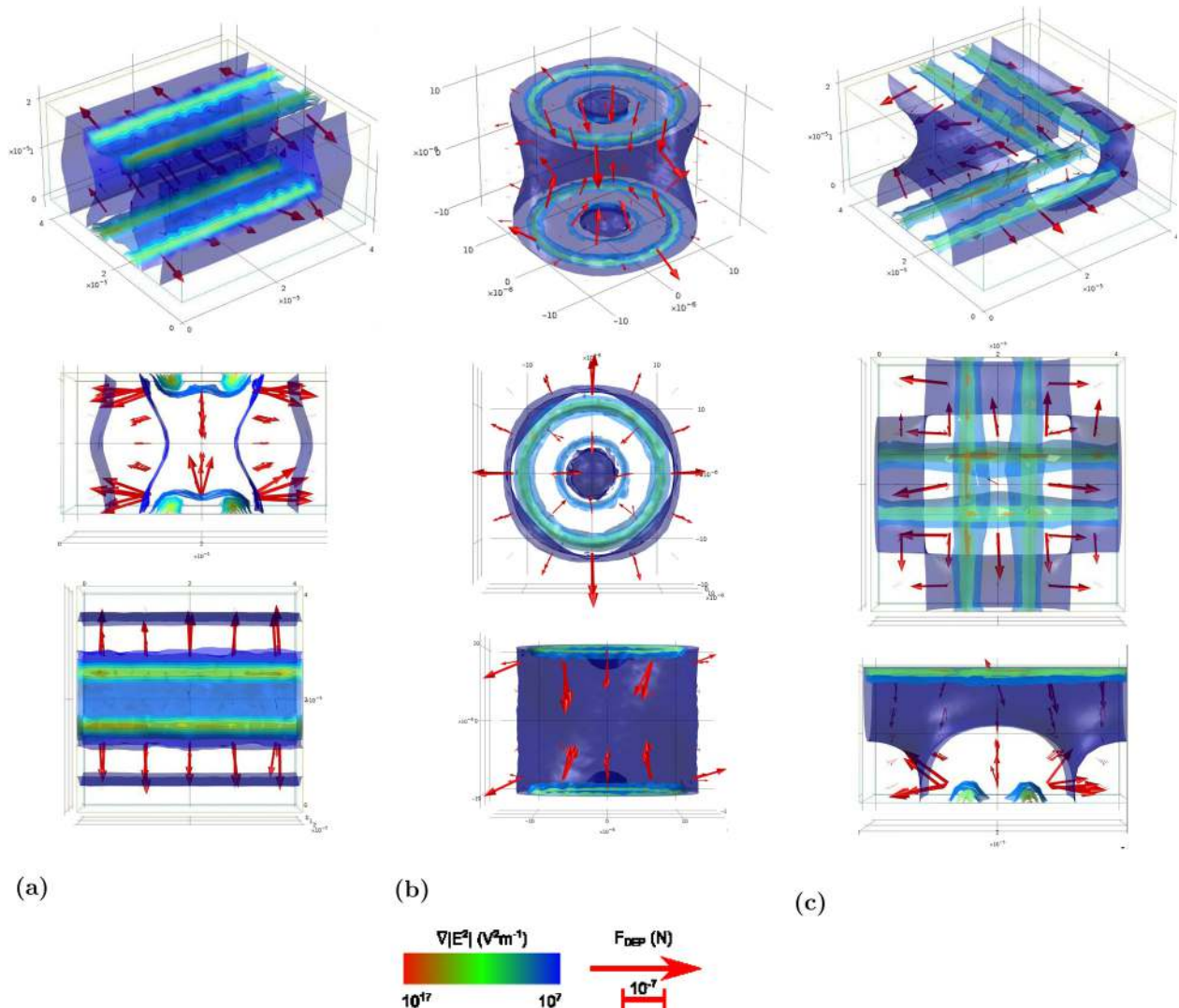


FIG. 4. 3-D electromagnetic simulations for (a) Parallel bars with face-to-face  $10\ \mu m$  bar electrodes, (b) Donut Trap with  $15\ \mu m$  as the inner trap diameter, and (c) Perpendicular bars with  $10\ \mu m$  perpendicular bars electrodes.



## B. Simulations: Electrokinetics regimes

### 1. Individual forces

For each design, we visualise the streamlines induced by each electrokinetic force (ACEO, ETE, or DEP) on  $1\ \mu\text{m}$  PS particles for each value of the parameters (particle diameter, conductivity of buffer, frequency, voltage). Fig. 5 plots the cross-section of the microchannel for the PaB design and Fig. 13 in Appendix A extends the plot for all designs. We can observe that those electrokinetic effects can induce 3 types of behaviours that will affect the particles movement.

- *Attractive and Convective Rolls (ACR)*: Typical ACEO flows at low frequencies ( $f < 5\ \text{kHz}$ ) and low conductivities ( $\sigma_m < 10^{-2}\ \text{S/m}$ ) are presented for the parallel bars design. Convection rolls at the edges of the electrodes force the position of the particle to the middle of both electrodes. Counter vortices can also be seen out of the electrodes and will drag particles far from the electrodes. According to the example given in Fig. 12 of Appendix A, tangents electric fields  $E_t$  magnitudes are in the order of  $1\ \text{MV/m}$  and decrease with the distance to the electrode. Moreover, the sign of  $E_t$  changes from one edge of the electrode to the other. This also implies a change in the direction of the velocity of the ACEO induced flow: resulting flow will be rolls pushing liquid to or from the edges to the center of the electrode.
- *Dispersive and Convective Rolls (DCR)*: The same type of vortices was observed for ETE flows with a change of direction when the  $\Pi$  factor is negative. We can, however, notice that ETE vortices are more centred on the electrode edges compared to ACEO ones. Particles are, therefore, repelled from electrodes borders with high speed from electrodes edges.
- *Electrodes Attraction or Repulsion (EAR)*: pDEP and nDEP patterns on the vertical bars design can either attract or repel particles from electrode borders. For the donut trap design, the directions of the forces are both towards the center of the trap and repelling from the outside border of the trap. This duality of direction should

provide an efficient way to localize particles in the center of the trap but also to repel non trapped particles far from the trap itself.

The axis of the forces will not change when changing the values of the frequency, the voltage or the medium conductivity but their direction and magnitude. Moreover, we have simulated three main motions of fluid and particles according to the effect from which they raised, which gives us the opportunity to identify the dominant force while observing particle motion during experiments.

### 2. Total forces exerted on particles

$F_{EHD}$  and  $F_{DEP}$  are summed in  $F_{Tot}$  as illustrated in Fig. 6 for a nDEP preferential regime. Hence, according to the geometry of the electrodes, particles will present different trajectories and their motions will get stabilized in a position relative to the electrodes according to  $F_{Tot}$  streamlines.

For the PaB design and under nDEP dominance conditions, particles are simply repelled from electrode borders but also confined in the center of the microchannel. For the DT design and still under nDEP dominance conditions, particles are focussed in the centres of the trap and of the channel itself.

When varying the parameters (frequency, voltage, particle diameter, and medium conductivity), a competition between forces appears. This competition will contribute in some cases to localize particles in the targeted areas or in other cases to push particles into undesired areas.

In order to understand this competition, a geometry dependant frequency-voltage mapping is presented in Fig. 7 and represents, for each COMSOL simulation, the magnitude of  $F_{Tot}$  exerted on a particle whose initial position is at the electrode edge. This cartography identifies the range of frequencies and voltages where an AC electrokinetic regime will dominate. It also determines the strength of the force applied on the particles.

$F_{Tot}$  is presented on those figures on which the white separation line show the balance  $F_{EHD} = F_{DEP}$ . One can

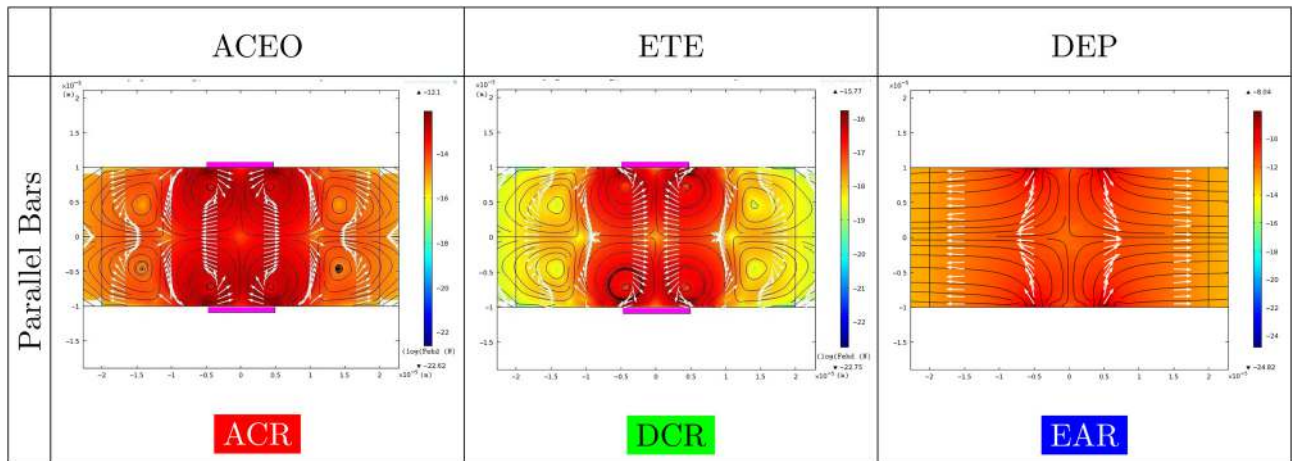


FIG. 5. Vectors and equipotentials of the dominant electrokinetic force exerted on PS  $1\ \mu\text{m}$  particles for the the PaB design under different conditions. Vectors are normalised and represented by the white arrows. Streamlines are represented in black and the spatial distribution of the magnitude of the force is plotted in the color background in the log scale (in Newton).  $F_{EHD}$  when ACEO dominates ( $\sigma_m = 2.10^{-4}\ \text{S/m}$ ,  $f = 1\ \text{kHz}$ ,  $V_{pp} = 10\ \text{V}$ ),  $F_{EHD}$  when ETE dominates ( $\sigma_m = 10^{-2}\ \text{S/m}$ ,  $f = 100\ \text{kHz}$ ,  $V_{pp} = 10\ \text{V}$ ),  $F_{DEP}$  in nDEP regime ( $\sigma_m = 2.10^{-4}\ \text{S/m}$ ,  $f = 2\ \text{MHz}$ ,  $V_{pp} = 10\ \text{V}$ ).



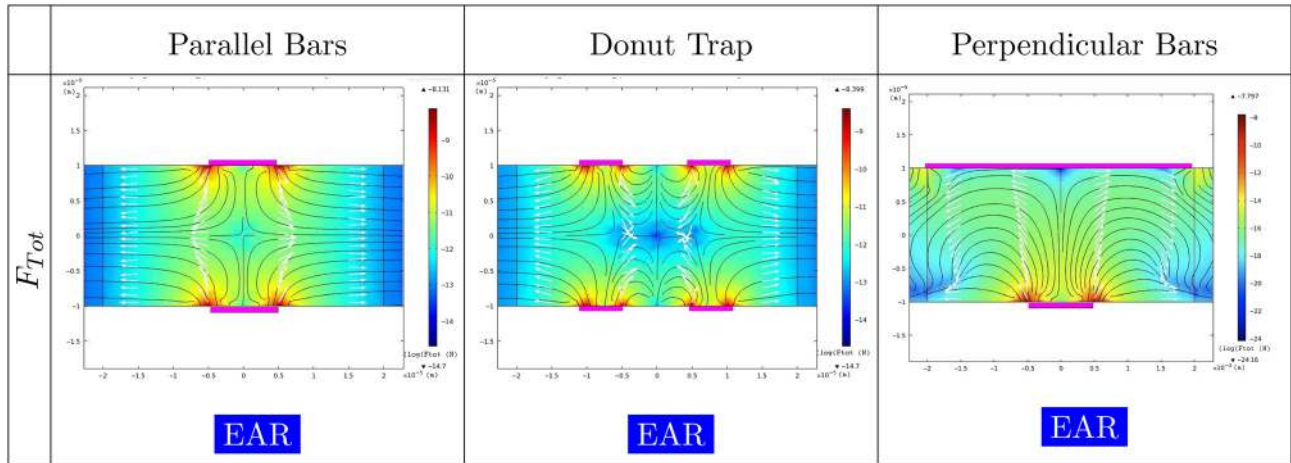


FIG. 6. Vectors and equi-potentials of the total electrokinetic force exerted on PS 1  $\mu\text{m}$  particles for the three designs. Vectors are normalised and represented by the white arrows. Streamlines are represented in black and the spatial distribution of the magnitude of the force is plotted in the color background in the log scale (in Newton).  $\sigma_m = 2 \times 10^{-4} \text{ S/m}$ ,  $f = 2 \text{ MHz}$ ,  $V_{pp} = 10 \text{ V}$ .

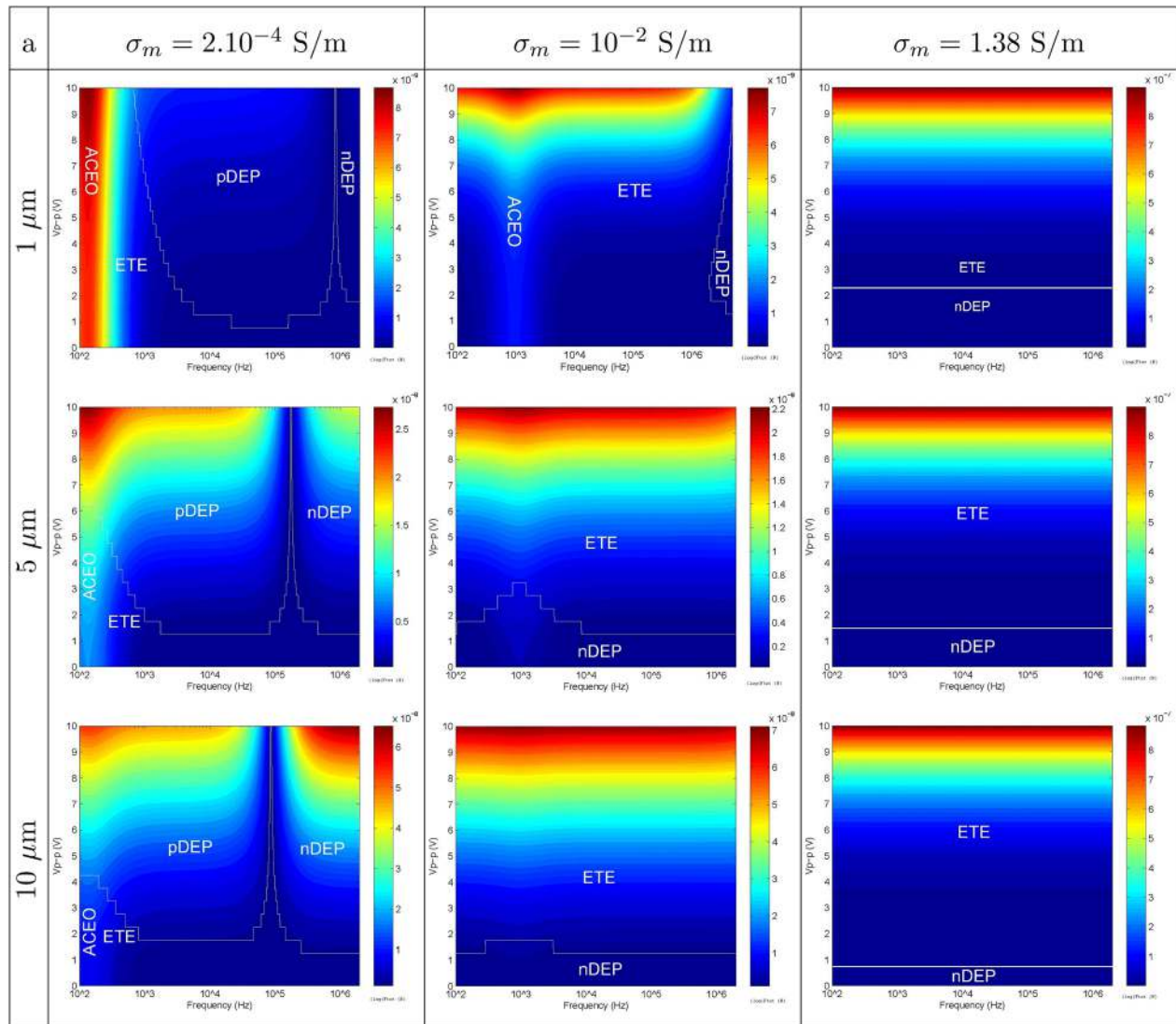


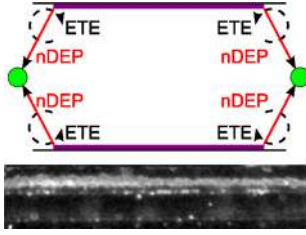
FIG. 7. Mapping of the total force exerted on the PS particles (diameter  $a$ ) for several frequencies and voltages. The magnitude of the total force (in Newton) exerted on this particle is simulated at the electrode edge and reported in each plot for each value of the studied parameters. The white separation lines represent the equilibrium point at which EHD and DEP forces are balanced.

TABLE I. Details of the electrokinetic regimes with their experimental observations.

Regime	Frequency	Conductivity (S/m)	Observations
Regime 1	$f < 10$ kHz	$\sigma_p = 2 \times 10^{-4}$	<p><b>Electrode center collection (ACEO and pDEP)</b></p> <p>Particles are concentrated in the center of upper and lower electrodes. Particles are under a strong ACEO regime. Raising the voltage increases the number of particles with a drag of particles that are far from electrodes. For all designs, particles are placed in the middle of the electrodes themselves. They remain in this position as long as the potential is applied. pDEP seems sufficiently strong to avoid particle to move in convective patterns. In the case of perpendicular bars design, particles accumulation appears only at the intersection between top and lower electrodes. Long range attraction to high concentrated zone is still present. One can notice no special motion at those frequencies for high conductivities, probably because ACEO velocities are not high enough to induce motion of liquid as shown in Fig. 1(b). Streamlines of liquid can be observed in Fig. 5 of Appendix B.4, where vortexes and counter vortexes of liquid on each electrodes can be observed</p>
Regime 2	$f = 1$ kHz	$\sigma_p = 10^{-2}$	<p><b>Electrode edge collection with stable position (ACEO and nDEP)</b></p> <p>Particles accumulate both at the center and at the edges of electrodes. Those behaviours are explained by the presence of ACEO at this range of frequency. Accumulation at the edge could suggest a pDEP response but not at this conductivity. The edge collection is the result of ACEO convective pattern against nDEP reaction that occurs only at the edges of electrodes. This is clearly observed on parallel bars. Contrary to the first accumulation process, particles are moving along the center of the electrodes. This latter behaviour emphasizes the competition between ACEO and nDEP. From the side, particles are located at the edges of the electrodes and convective rolls are observed on the lower right hand of Fig. 5 in Appendix B.4</p>
Regime 3	$f = 50$ kHz, $f = 500$ kHz	$\sigma_p = 2 \times 10^{-4}$	<p><b>Electrode edge collection with convection rolls (pDEP and ETE)</b></p> <p>Particles are collected at the edges of electrodes with a clear convective motion as showed in Fig. 5 of Appendix. At those frequencies, particles are under pDEP regime but ETE drags the particle among rolls. This effect is increased when the voltage is raising. At higher voltages, the <math>\Pi</math> factor of the ETE changes its sign and convective rolls tend to repel particles from the electrode edges.</p>
Regime 4	$f = 50$ kHz	$\sigma_p = 10^{-2}$ , $\sigma_p = 1.38$	<p><b>Electrode edge collection with convection rolls and chain formation (weak nDEP and ETE)</b></p> <p>At mid-high conductivities and for, particles are attracted to electrodes edges and started to form particles chain. This behaviour has been observed<sup>11,58</sup> in coplanar electrode configuration. Chains of particles appear both in the plane of the lower and upper electrodes but also between electrodes themselves. In the case of nDEP, particles chain formation is the results of attraction inter-particles due to low electric field strength between them.<sup>24</sup> It can be noticed that chain formation does not appear for the donut trap or the perpendicular bars designs. In those cases, particles are attracted to the outer edges of electrodes. Those observations confirm that this regime results from a competition between ACEO and ETE forces.<sup>24</sup> In the parallel bars design, EHD forces are symmetrical and have the same convection rolls patterns on both sides of the electrodes, as discussed later. This symmetrical behaviour results in the attraction of particles before and after the electrodes and between themselves. In the other designs, EHD flow patterns are not symmetrical and particles that are "far" from regions where the gradient are the strongest are not submitted to any forces. Particle chains are clearly observed in the X-Z plan in Fig. 5 of Appendix B.4 where chains are aligned along the z axis</p>
Regime 5	$f = 500$ kHz, $f = 2$ MHz	All, low voltages	<p><b>Collection in front of electrode with stable position (strong nDEP dominant)</b></p> <p>At high frequencies, particles are repelled from electrodes borders. A single line alignment can be observed for vertical bars. For the donut trap design, 2 behaviours are observed, first particles are focused in the center of the traps, i.e. repelled from the inside borders of the trap, but also they are repelled from the trap itself, i.e. from the outside border of the trap. This dual behaviour emphasizes the trapping efficiency of the donut trap. For the perpendicular bars design, particles are placed between vertically aligned electrodes. All those behaviours suggest an nDEP regime without any convective rolls. When the voltage is increased, rolls start to appear. As particles are repelled from the electrodes, they are located in the center of the microfluidic channel (in the middle plane X-Z) as shown in Fig. 5 of Appendix B.4</p>

TABLE I. (Continued.)

Regime	Frequency	Conductivity (S/m)	Observations
Regime 6	$f = 500 \text{ kHz}, f = 2 \text{ MHz}$	All, high voltages	<p><b>Collection in front of electrode with convection rolls (strong nDEP and ETE)</b></p> <p>In this last regime, particles are repelled from electrodes at high frequencies. But when raising the voltage, convective rolls tend to drag and accumulate long range particles to the electrode borders. Those particles are then repelled by nDEP and so on. Convective rolls assist nDEP to make a strong barrier in the case of parallel bars, even when particles are submitted to a hydrodynamic drag flow. For the donut trap design, the same behaviours as the Regime 5 are observed but with more strength: particles seem to be more centred within the donut trap and more repelled from its outside border. For the perpendicular bars design, particles are still repelled from the activated electrodes and localized between the vertical ones. However, in order to maintain a precise localisation within the perpendicular bars design, it is most likely that the adjacent electrode should be also activated since convective rolls tend to repeat particles from the electrode as far as not feeling the electrokinetics forces any more. Fig. 5 of Appendix B.4 shows the lateral view of the Regime 6 in the donut trap design. Particles are centred in the middle of the channel but convective rolls can be seen on lower electrodes</p>



clearly see the domination of ACEO at low frequencies and the CMF like curvature of the DEP responses at the pDEP-nDEP interface. For each domain, the dominant force has been overlaid and matches with the experimental behaviours for all designs. Such mappings are presented with the total forces when raising particle diameter and medium conductivity. More generally, ETE dominates at high conductivities but a nDEP window remains opened at low voltages.

Those simulations and mappings allow the extraction of several frequency-voltage couples for which dominant behaviours seem to appear. For example, at  $\sigma_m = 2 \times 10^{-4}$  S/m a typical (f,V) couple may be  $f = 2 \text{ MHz}$ ,  $V_{pp} = 10 \text{ V}$  in order to induce a nDEP motion of particles. We started from the values of those couples to experimentally observe the particles' behaviours within the microfluidic chips for the 3 electrodes geometries.

### C. Experimental: Electrokinetics regimes

We then observe and identify the electrokinetic regimes that govern the particles displacements within the microfluidic chip. The three electrodes geometries previously presented are tested with PS particles (diameter  $1 \mu\text{m}$ ) suspended in different media. This size (the smallest of our range of experiments) is chosen because small particles present the weakest DEP response and allow a better understanding of the competition with the others EHD forces. Identical behaviours are expected with the biggest PS particles (diameters 5 and  $10 \mu\text{m}$ ) but with stronger DEP forces.

For each conductivity, several key frequencies have been selected from the simulations results according to the strength of each force: ACEO frequency ( $f = 1 \text{ kHz}$ ), pDEP and negative ETE frequency ( $f = 50 \text{ kHz}$ ), positive ETE frequency ( $f = 500 \text{ kHz}$ ), nDEP and positive ETE frequency ( $f = 2 \text{ MHz}$ ). In the same way, 3 voltages have been selected: 2, 5, and 10 V. Note that for high conductivities, 10 V is not applied to avoid electrolysis of water and electrode degradation.<sup>46</sup>

In general, at a given frequency, we observe that increasing the voltage leads to a stronger force that was already dominating. However, in some cases, the presence of forces in

competition leads to a contribution of each individual force. For all electrodes designs, we observe several similar particles motions in the X-Y plane. We have identified six typical behaviours, further referred as the different *regime*. Table I describes the experimental observation of each regime and detailed pictures for each design are presented in Table II of Appendix B for parallel trap electrodes, Table III of Appendix B for donut trap, and Table IV of Appendix B for perpendicular electrodes (mDEP) configuration. Each regime has been outlined with a specific color and we detail a schematic explanation of the motion of the particles. Moreover, for each regime, the localizations of particles were observed laterally in the X-Z plane for the donut trap geometry only and observations are shown in Table V of Appendix B.

This parametric study demonstrates experimentally the 6 dominant electrokinetic regimes that can be exploited in the microfluidic chip with 3-D bi-layer electrodes configurations. Each regime is a combination of electrokinetic forces, whose individual streamlines were simulated in Sec. IV B, that superimpose and induce a localization of the particles in a stable position at which the forces reach a balance. Hence, we emphasize that the localizations of the particles relatively to the electrodes are the result of a competition between EHD and DEP forces. According to where the particles need to be localized, each regime can be used independently. We will hence exploit the regime 5 (strong nDEP regime) to focusing the particles in the middle of the microfluidic channel and in front of the electrodes, as shown in Fig. 8.

This regime will be exploited in the next section to realize electro-microfluidic functions for particle handling in a purely 3-D electrodes geometry.

### D. Electrokinetic functions

We have chosen to investigate the capacity of the parallel bar and donut trap to manipulate colloidal particles under constant flow rates. We introduce electrokinetic functions for handling particles based on the design of those bi-layer electrodes. The principle of those electro-microfluidic functions is first exposed and then experimentally tested. Each function is based on the use of higher regimes (5 or 6) because those



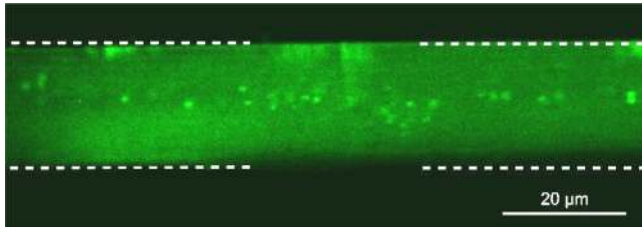


FIG. 8. Lateral observation (X-Z plane) of the particles displacement for the donut trap design at  $f=500$  kHz,  $f=2$  MHz,  $\sigma_p = 2 \times 10^{-4}$  S/m. The electrodes are highlighted in dashed lines.

regimes have been observed in high conductivity medium and can be exploited within cell culture medium.

### 1. Stop function with parallel bars

Parallel bars electrodes that are perpendicular to the channel are exploited to sort particles and provide a stop function based on the CMF crossover frequency. Dragged by a hydrodynamic flow inside the microfluidic channel thanks to the fluidic module of the platform, the particles are stopped by a strong nDEP force in front of the electrodes as illustrated in Fig. 9(a) and observed by the regime 5 motion of particles. When increasing the voltage at a constant flow rate of incoming colloids, more particles are stopped. We define the stop efficiency as the ratio between the number of incoming colloids and the number of unstopped particles by the nDEP trap.

Fig. 9(b) shows the evolution of the stop efficiency at a constant flow rate ( $Q = 500$  pl/s) when raising voltage for different medium conductivities. We recall that the section of the microfluidic channel is  $500 \times 20 \mu\text{m}$ . All the flow

rates in this section have been directly measured by tracking the velocities of particles inside the microfluidic channel before the electrodes area.

A threshold voltage is observed before the stop efficiency starts to raise (4 V at low conductivity and 9 V at high conductivity). This threshold value represents the minimum DEP force that is needed to counteract the particle flow drag force. At high voltages (above  $>10$  V), a plateau region is reached above 95% of the stop efficiency function. The minimum voltage that is required to reach this region increases when raising the medium conductivity. In this area, the DEP and ETE forces overpower the drag force and all particles are stopped.

The efficiency of the stop function is also evaluated in terms of maximum sustainable flow rate according to the electrokinetic regime. Hence, a high voltage is applied (typically 20 V) to reach the previous 95% stop function efficiency regime and the AC frequency is swept in order to change the electrokinetic regime. After applying the voltage, the flow rate is raised until all previously repelled particles are dragged. Fig. 9(c) plots the maximum sustainable flow rate until no particles are trapped any more.

At low conductivity, when the AC frequency is lower than the crossover frequency ( $f < f_0 = 1.1$  MHz), pDEP occurs but also ETE. As viewed in previous paragraph, ETE force is dominant, forcing the particles to be repelled from the electrodes, but pDEP contributes also to attract particles to the electrodes. This competition is unbalanced in favour of ETE force when raising the frequency and thus the maximum sustainable flow rate gets higher. When  $f > 1.1$  MHz, particles displacement is governed by nDEP forces which add a contribution to the ETE forces. Both of them repel

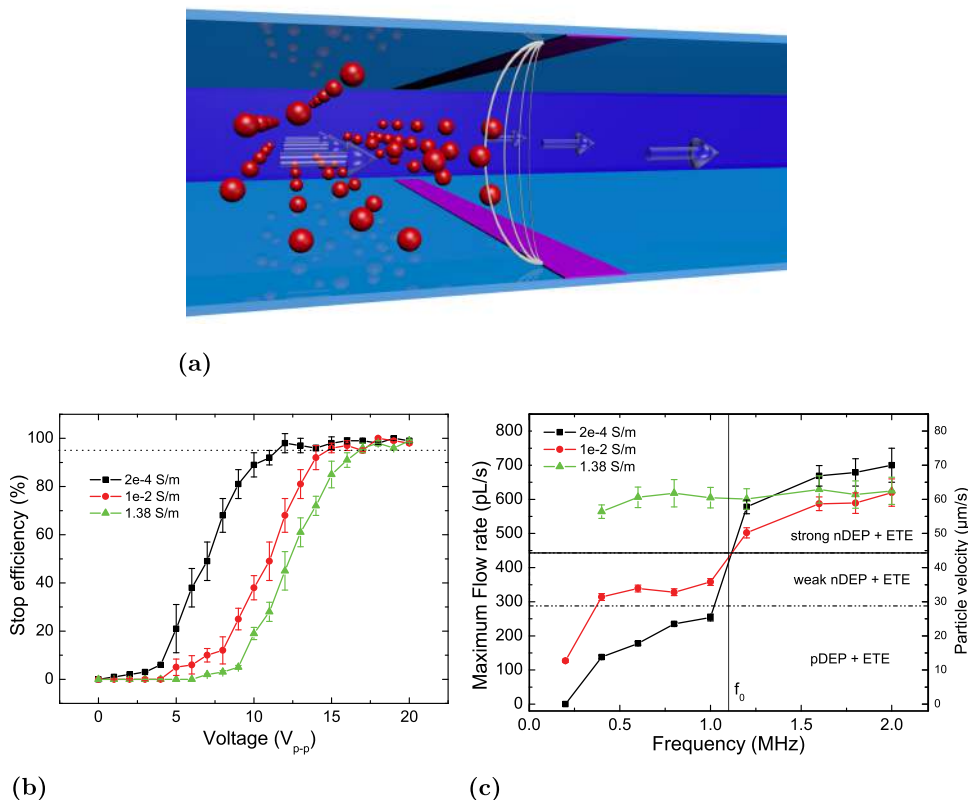


FIG. 9. (a): Illustration of the stop function. The red colloidal particles are stopped in front of the parallel bars electrodes set in the regime 5 (strong nDEP dominant). (b): Efficiency of stop function with the parallel bars design for  $1 \mu\text{m}$  PS particles and different medium conductivities (nDEP regime with  $f = 2$  MHz) at a constant flow rate of  $Q = 500$  pl/s. The dashed line represents 95% of efficiency. (c): Maximum flow rate of the stop function with the parallel bars electrodes (20 V and  $f = 2$  MHz) design for different medium conductivities and  $1 \mu\text{m}$  PS particles. The particle velocity is directly converted from flow rate according to the microchannel dimensions and corresponds to the velocity of particles that arrive in front of the trap without going through.



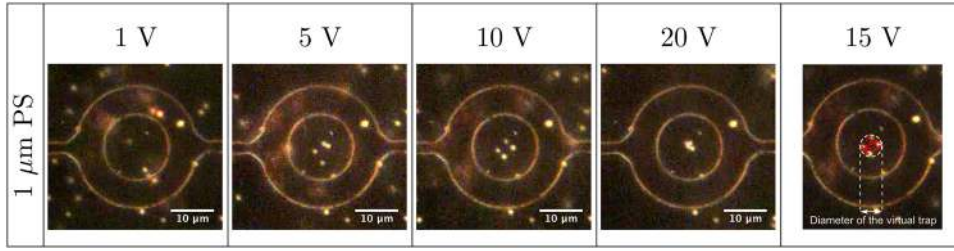


FIG. 10. Photographs of  $1\ \mu\text{m}$  PS particles in the donut trap at  $f=2\ \text{MHz}$  and raising voltages. Particles motions are confined in the nDEP cage whose diameter is reducing as enhancing the applied voltage value. The last picture is an example of particle displacement tracking used to determine the diameter of the virtual trap.

particles from electrodes and maximum sustainable flow rate reaches a maximum when nDEP is fully maximized.

At medium conductivity, as can be seen in Fig. 1(a), particles are under a weak (i.e.,  $\text{Re}[CMF(\omega)] > -0.5$ ) nDEP regime that adds a small contribution to ETE forces. When raising the frequency, nDEP becomes stronger and reaches the strong nDEP and ETE regime. At high conductivity, particles are directly in the maximum sustainable regime because the absolute value of their  $\text{Re}[CMF(\omega)]$  is already at maximum. This explains the green-triangle plateau.

Finally, we show that the 3-D parallel bars electrodes design used in a nDEP regime for  $1\ \mu\text{m}$  PS particles can sustain a flow up to 600 pl/s in the microfluidic channel. The right hand of the legend indicates the velocity of particles that inbound the trap without penetrating through it. Those particles fall outside of the trap to finally being dragged by the laminar flow between the electrodes trap and the microchannel. From those observations and according to the simulations in Sec. IV B, we can assert that the stop function will provide a higher stop efficiency when increasing the particle diameter.

## 2. The trap function with donut trap

First, the localisation of the particles in the center of the channel (X-Z plane) was observed for several sizes of

particles at high frequency ( $f=2\ \text{MHz}$ ) and high voltage ( $V_{p-p}=20\ \text{V}$ ) as presented in Fig. 14 of Appendix C.

Then, we focused on the capacity of the donut trap to focus particles in the center of the donut. Hence,  $1\ \mu\text{m}$  PS particles were trapped under nDEP conditions ( $f=2\ \text{MHz}$ ) in DI water with raising voltages. As can be seen in Fig. 10, the trap function creates a virtual trap cage. The size of this virtual cage in the X-Y plane is reduced when the strength of the nDEP force is increased by the applied voltage. Under those conditions, particles Brownian motion is confined within the nDEP cage. The behaviour of larger particles has also been observed and is presented in Fig. 15 of Appendix C.

The virtual trap cage diameter has been quantified by averaging the maximum displacement coordinates of the trapped particles relatively to the center of the donut trap, as shown in Fig. 10 ( $1\ \mu\text{m}$  PS, 15 V). This value is quantified for each voltage and conductivity. Fig. 11(a) gives the virtual trap cage diameter for  $1\ \mu\text{m}$  particles in the 3 buffer solutions. Under nDEP conditions, as the voltage increases, the virtual trap cage gets more confined. A plateau region is observed at high voltages defining the minimum virtual trap cage diameter.

Fig. 11(b) plots the minimum virtual trap cage diameter for 1, 5, and  $10\ \mu\text{m}$  PS particles in the different buffer solutions. The minimum trap diameter line represents the diameter of the particle itself. Small particles can be trapped at

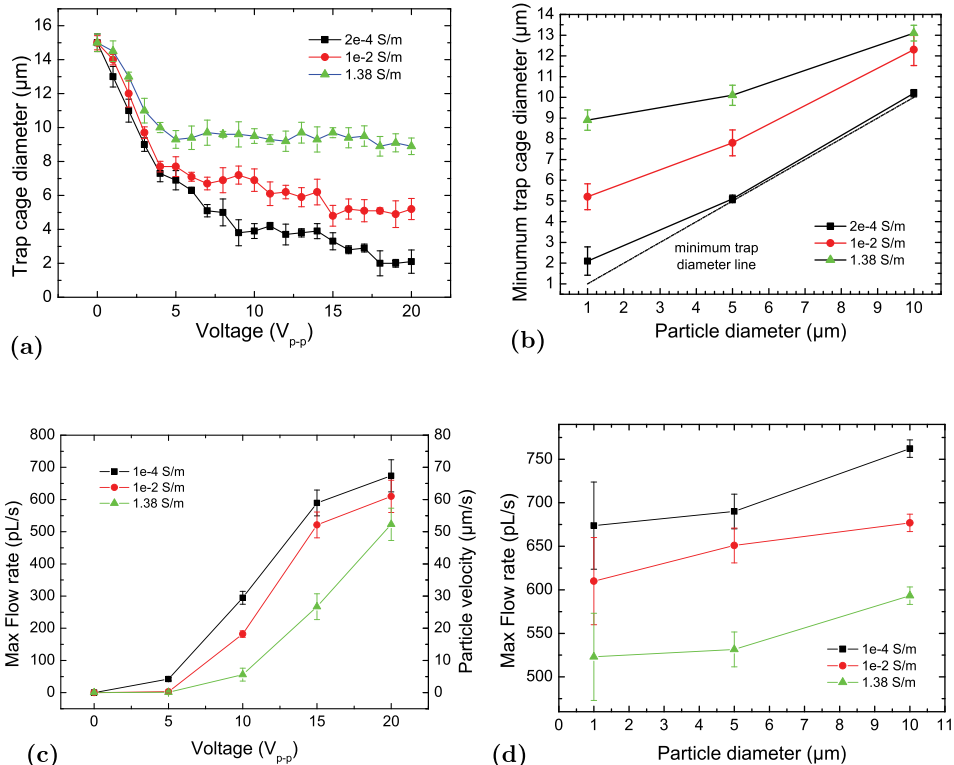


FIG. 11. (a): Effective diameter of the virtual trap cage for  $1\ \mu\text{m}$  PS particles when varying voltage and medium conductivity. (b): Minimum virtual trap cage diameter for  $1\ \mu\text{m}$ ,  $5\ \mu\text{m}$ , and  $10\ \mu\text{m}$  PS particles for several medium conductivities. (c): Maximum sustainable flow rate for  $1\ \mu\text{m}$  PS particles in the donut trap when varying voltage and conductivity. Particle velocity is directly converted from flow rate according to the microchannel dimensions. (d): Maximum value of the sustainable flow rate for  $1\ \mu\text{m}$ ,  $5\ \mu\text{m}$ , and  $10\ \mu\text{m}$  PS particles when varying voltage and conductivity. Particles traps in the donut trap cage ( $f=2\ \text{MHz}$  and  $V_{p-p}=20\ \text{V}$ ) are still trapped in the cage until those flow rates.

single level only in low conductivity buffers. Bigger particles can also be trapped at a single level and maintained in the trap for high conductivity buffers, since the minimum diameter of the cage is lower than twice the diameter of the particle itself. Those experiments demonstrates the capacity of the donut trap design to maintain in 3-D cells of 5 to 10  $\mu\text{m}$  diameter in their cell culture medium.

Finally, we investigated the capacity of the donut traps to sustain flow whilst particles were trapped. The following experiments were conducted: Once particles were trapped under high frequencies ( $f=2$  MHz), the voltage was tuned up and the drag flow was enhanced. As soon as the particle was released from the trap, flow rate was stopped and denoted as the maximum sustainable flow rate. Experiments were conducted with 1  $\mu\text{m}$  PS particles in each buffer solution and results are presented in Fig. 11(c).

At first, a threshold voltage value is required to maintain particles in the trap. At maximum voltage (20 V), flow up to 650 pl/s can be sustained while maintaining the particles in the trap. Generally, more voltage implies more sustainable flow rate. Therefore, 1, 5, and 10  $\mu\text{m}$  PS particles were trapped with  $f=2$  MHz and  $V_{p-p}=20\text{V}$  and the flow rate was increased until the particle was released from the trap. Fig. 11(d) presents the maximum sustainable flow rates at several conductivities.

The maximum sustainable flow rates are in the same order of magnitude for each medium. As presented in the precedent section, ETE forces can be significant for high voltages and seem to overpower DEP responses of particles at high voltages. Hence, thanks to the coupling of ETE and nDEP, particles can be trapped and sustained with flow up to 600 pl/s.

To conclude, we have demonstrated 2 main functions for colloidal handling in microfluidic channels under hydrodynamical flows. The barrier like stop function can be maintained more than 95% of incoming particles in a deterministic position along the microchannel while

injecting liquid medium up 750 pl/s in a large range of medium conductivities. Moreover, the donut trap design extends this possibility to a 3-D deterministic positioning of particles in the center of the microchannel. Particles can be trapped at a very precise location relatively to the center of the donut trap and maintained at this position for incoming flows up to 750 pl/s. The holding flow rates of our microfluidic chip show a real benefit compared with the state-of-art results. Regarding the particle trap resistance to the incoming flow, the bi-layer electrodes donut trap function demonstrates at least a factor two with the holding force of co-planar quadrupole design<sup>25</sup> or co-planar pDEP trap,<sup>59</sup> and a decade more with the one of nDEP co-planar electrodes.<sup>48</sup>

## V. CONCLUSIONS

We have presented a complete study of the electrokinetic regimes that govern the manipulation of particles under 3-D non-uniform AC electric field in low to high conductivities medium. The bi-layer electrodes microfluidic chip offers the possibility to design microfluidic functions: The stop function with parallel bars electrodes, the trap function with donut trap, and the 3-D localization with perpendicular bars. Numerical simulations have detailed the impact of EHD or DEP force on particle displacements. Map of the dominant electrokinetic regime has been determined in a broad range of frequencies, voltages, and medium conductivities. Moreover, experiments demonstrate that 1, 5, and 10  $\mu\text{m}$  PS particles can be precisely trapped in 3-D under a liquid flow up to 600 pl/s, a clear benefit compare to standard 2-D electrodes designs. Unlike coplanar electrodes where EHD forces can have undesired localisation of particles, 3-D electrodes offer the capacity to take advantage of those forces. Future work will focused on the implementation of biological samples for cells manipulation by DEP within this 3-D microfluidic chip.

## APPENDIX A: SIMULATIONS RESULTS

### 1. Simulations of the tangent electric field

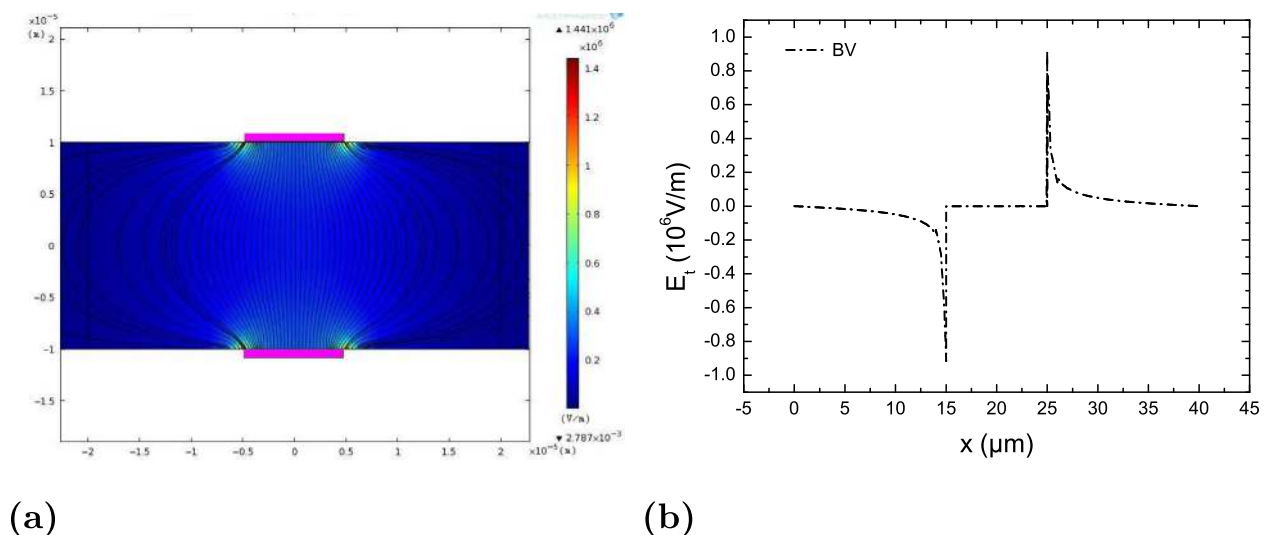


FIG. 12. (a): Spatial distributions of  $|E|$  (V/m) and equipotentials for the Parallel bars design when  $\sigma_m = 2 \times 10^{-4}$  S/m,  $f=1$  kHz and  $V_{pp} = 10$  V. (b): Simulated tangents electric field associated.

**2. Vectors and equi-potentials of the dominant electrokinetic force**

Vectors and equi-potentials of the dominant electrokinetic force exerted on PS 1  $\mu\text{m}$  particles for the 3 bi-planar designs under different conditions. Vectors are normalised and represented by the white arrows. Streamlines are represented in black and the spatial distribution of the

magnitude of the force is plotted in the color background in the log scale (in Newton). From top to bottom:  $F_{EHD}$  when ACEO dominates ( $\sigma_m = 2.10^{-4} \text{ S/m}$ ,  $f = 1 \text{ kHz}$ ,  $V_{pp} = 10 \text{ V}$ ),  $F_{EHD}$  when ETE dominates ( $\sigma_m = 10^{-2} \text{ S/m}$ ,  $f = 100 \text{ kHz}$ ,  $V_{pp} = 10 \text{ V}$ ),  $F_{DEP}$  in nDEP regime ( $\sigma_m = 2.10^{-4} \text{ S/m}$ ,  $f = 2 \text{ MHz}$ ,  $V_{pp} = 10 \text{ V}$ ), and  $F_{Tot}$  in nDEP regime ( $\sigma_m = 2.10^{-4} \text{ S/m}$ ,  $f = 2 \text{ MHz}$ ,  $V_{pp} = 10 \text{ V}$ ).

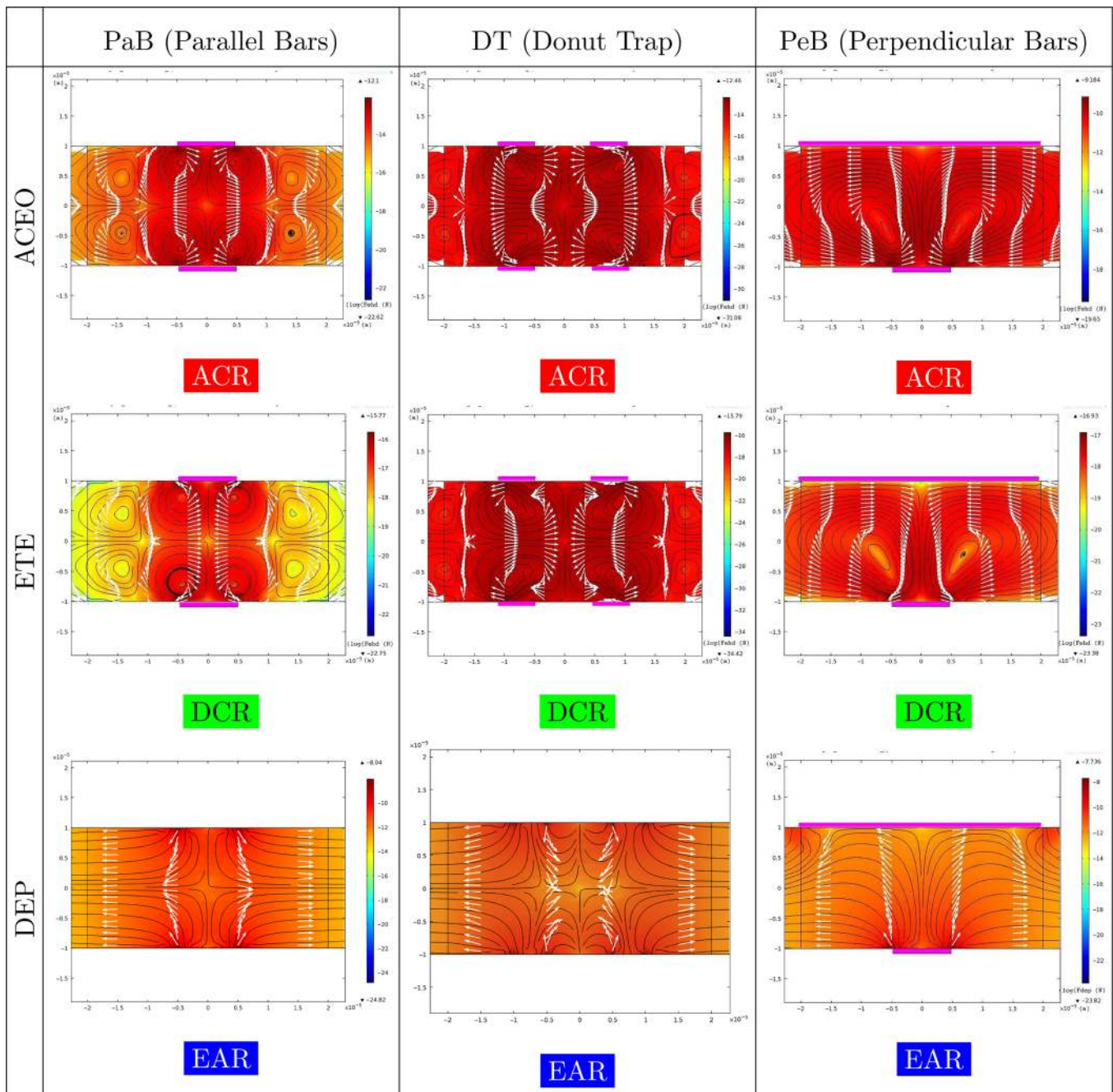


FIG. 13. Vectors and equi-potentials of the dominant electrokinetic force exerted on PS 1  $\mu\text{m}$  particles for the 3 bi-planar designs under different conditions. Vectors are normalised and represented by the white arrows. Streamlines are represented in black and the spatial distribution of the magnitude of the force is plotted in the color background in the log scale (in Newton). From top to bottom:  $F_{EHD}$  when ACEO dominates ( $\sigma_m = 2.10^{-4} \text{ S/m}$ ,  $f = 1 \text{ kHz}$ ,  $V_{pp} = 10 \text{ V}$ ),  $F_{EHD}$  when ETE dominates ( $\sigma_m = 10^{-2} \text{ S/m}$ ,  $f = 100 \text{ kHz}$ ,  $V_{pp} = 10 \text{ V}$ ) and  $F_{DEP}$  in nDEP regime ( $\sigma_m = 2.10^{-4} \text{ S/m}$ ,  $f = 2 \text{ MHz}$ ,  $V_{pp} = 10 \text{ V}$ ).



**APPENDIX B: EXPERIMENTAL OBSERVATION OF THE ELECTROKINETIC REGIMES**

**1. The parallel bars**

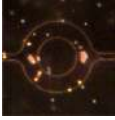
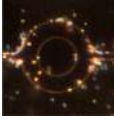
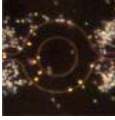
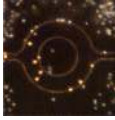
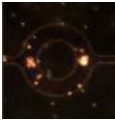
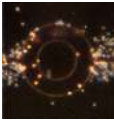
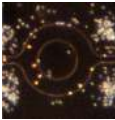
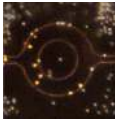
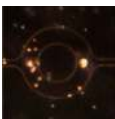
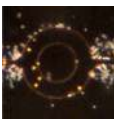
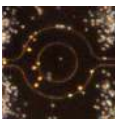
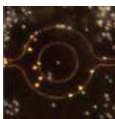
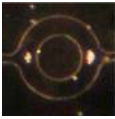
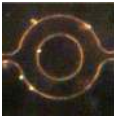
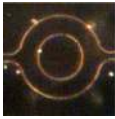
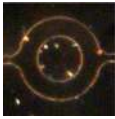
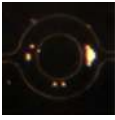
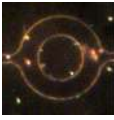
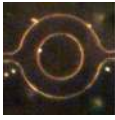
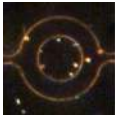
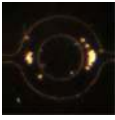

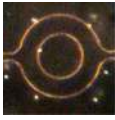
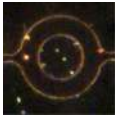
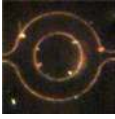
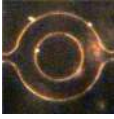
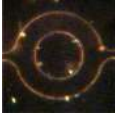

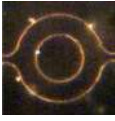

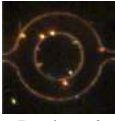
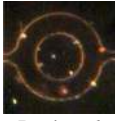
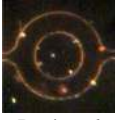
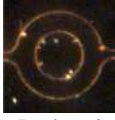
TABLE II. Parallel bars electrodes: Identification of AC electrokinetics regimes.

$\sigma_m$	V	Frequency			
		1 KHz	50 KHz	500 KHz	2 MHz
$2 \times 10^{-4}$ S/m	2 V	  Regime 1	  Regime 3	  Regime 3	  Regime 5
	5 V	 Regime 1	 Regime 3	 Regime 3	 Regime 5
	10 V	 Regime 1	 Regime 3	 Regime 3	 Regime 6
	$10^{-2}$ S/m	2 V	  Regime 2	  Regime 4	  Regime 5
5 V		 Regime 2	 Regime 4	 Regime 6	 Regime 6
10 V		 Regime 2	 Regime 4	 Regime 6	 Regime 6
1.38 S/m		2 V	  Regime 5	  Regime 5	  Regime 5
	5 V	 Regime 5	 Regime 5	 Regime 6	 Regime 6
	10 V	X	X	 Regime 6	 Regime 6



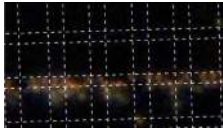
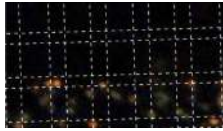
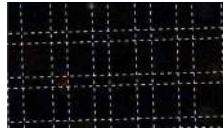
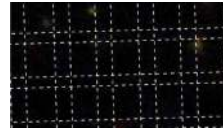
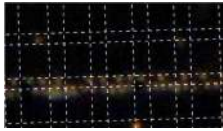
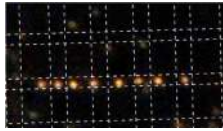
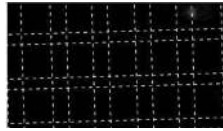
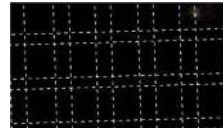
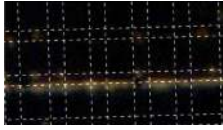


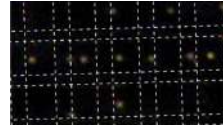
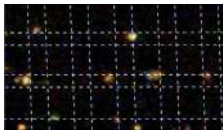
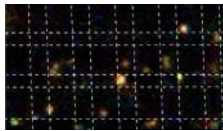
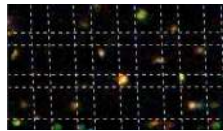
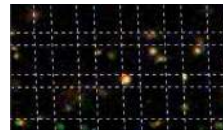
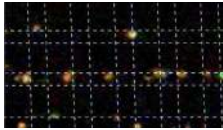
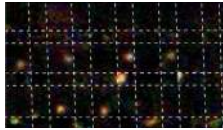
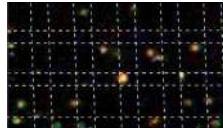
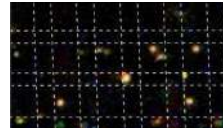
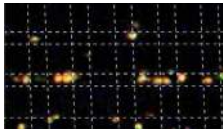
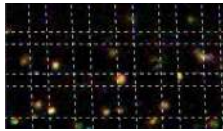
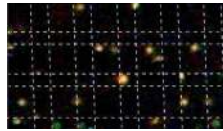
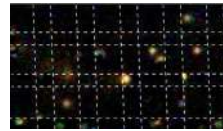
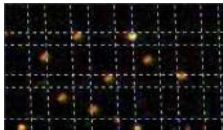

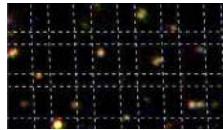
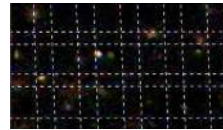
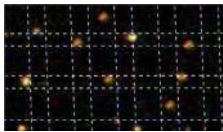
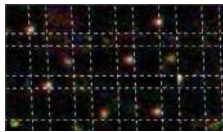
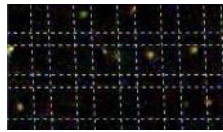
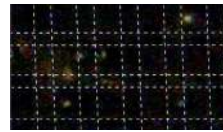
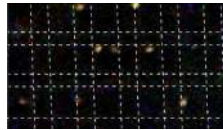
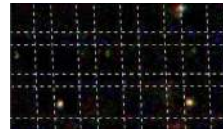
**2. The donut trap**

TABLE III. Donut trap: Identification of AC electrokinetics regimes.

$\sigma_m$	V	Frequency			
		1 KHz	50kHz	500 kHz	2 MHz
$2 \times 10^{-4}$ S/m	2 V	 Regime 1	 Regime 3	 Regime 3	 Regime 5
	5 V	 Regime 1	 Regime 3	 Regime 3	 Regime 5
	10 V	 Regime 1	 Regime 3	 Regime 3	 Regime 5
$10^{-2}$ S/m	2 V	 Regime 2	 Regime 4	 Regime 5	 Regime 5
	5 V	 Regime 2	 Regime 4	 Regime 6	 Regime 6
	10 V	 Regime 2	 Regime 4	 Regime 6	 Regime 6
1.38 S/m	2 V	 Regime 2	 Regime 4	 Regime 5	 Regime 5
	5 V	 Regime 2	 Regime 4	 Regime 6	 Regime 6
	10 V	X	X	 Regime 6	 Regime 6

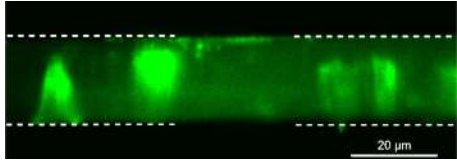
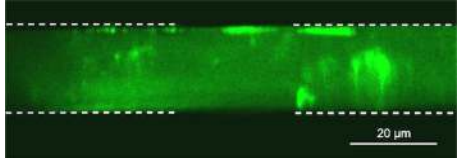
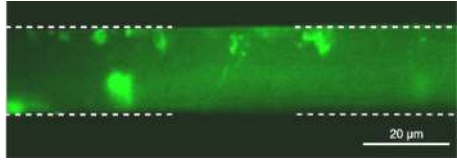
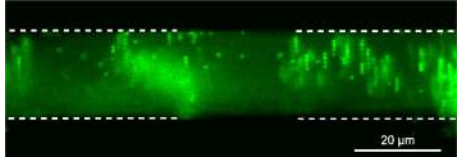
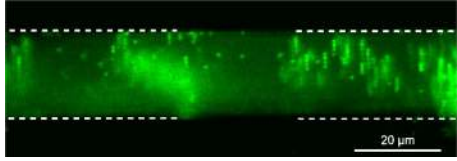
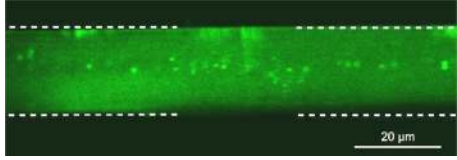
### 3. The perpendicular bars

TABLE IV. Perpendicular bar electrodes: Identification of AC electrokinetics regimes.

$\sigma_m$	V	Frequency			
		1 KHz	50 kHz	500 kHz	2 MHz
$2 \times 10^{-4}$ S/m	2 V	 Regime 1	 Regime 3	 Regime 3	 Regime 5
	5 V	 Regime 1	 Regime 3	 Regime 3	 Regime 6
	10 V	 Regime 1	 Regime 3	 Regime 3	 Regime 6
$10^{-2}$ S/m	2 V	 Regime 2	 Regime 4	 Regime 5	 Regime 5
	5 V	 Regime 2	 Regime 4	 Regime 6	 Regime 6
	10 V	 Regime 2	 Regime 4	 Regime 6	 Regime 6
1.38 S/m	2 V	 Regime 2	 Regime 4	 Regime 5	 Regime 5
	5 V	 Regime 2	 Regime 4	 Regime 6	 Regime 6
	10 V	X	X	 Regime 6	 Regime 6

#### 4. From lateral side

TABLE V. Lateral observation (X-Z plane) of the particles displacement for the donut trap design. The electrodes are highlighted in dashed lines.

Regime	Frequency	Conductivity	Lateral observation
Regime 1	$f < 10$ kHz	$\sigma_p = 2 \times 10^{-4}$ S/m	Electrode center collection (ACEO and pDEP) 
Regime 2	$f = 1$ kHz	$\sigma_p = 10^{-2}$ S/m	Electrode edge collection with stable position (ACEO and nDEP) 
Regime 3	$f = 50$ kHz, $f = 500$ kHz	$\sigma_p = 2 \times 10^{-4}$ S/m	Electrode edge collection with convection rolls (pDEP and ETE) 
Regime 4	$f = 50$ KHz	$\sigma_p = 10^{-2}$ S/m, $\sigma_p = 1.38$ S/m	Electrode edge collection with convection rolls and chain formation (weak nDEP and ETE) 
Regime 5	$f = 500$ kHz, $f = 2$ MHz	All, low voltages	Collection in front of electrode with stable position (strong nDEP dominant) 
Regime 6	$f = 500$ kHz, $f = 2$ MHz	All, high voltages	Collection in front of electrode with convection rolls (strong nDEP and ETE) 

#### APPENDIX C: CHARACTERIZATION OF THE DONUT TRAP CAGE

In order to check the localisation of the particles in the channel (X-Z plane), experiments at high frequency ( $f = 2$  MHz) and high voltage ( $V_{p-p} = 20$  V) were conducted

for several sizes of particles in DI water with the side-view platform. Particles are focused in the center of the channel as they are repelled from the 4 electrodes borders as shown in Fig. 14.

$5 \mu\text{m}$  and  $10 \mu\text{m}$  PS particles have been placed in the donut trap at high frequencies ( $f = 2$  MHz) and the voltage was raised. The same behaviour as for the  $1 \mu\text{m}$  is observed



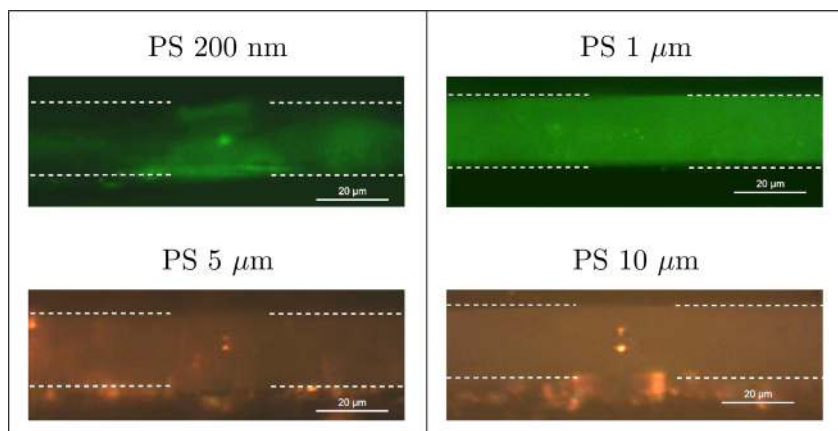


FIG. 14. Side-view pictures of the microfluidic channel with PS particles in the donut trap at  $f=2$  MHz and  $V_{p-p}=20$  V with raising particles diameters. For 5 and 10  $\mu\text{m}$  particles size, two spots are visible in the center of the channel. They correspond to the scattering of illuminated light on the upper and lower contours of the dielectric particles.

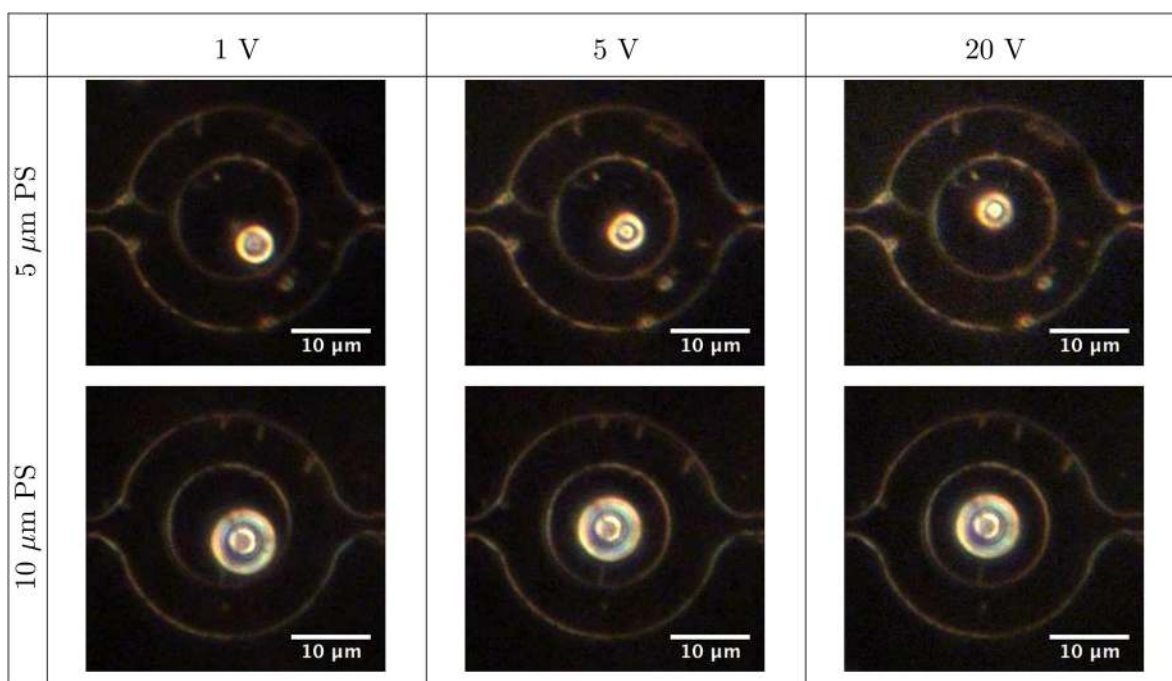


FIG. 15. Photographs of 5  $\mu\text{m}$  and 10  $\mu\text{m}$  PS particles trapped at  $f=2$  MHz and raising voltages. The nDEP cage diameter is getting smaller as the voltage increases implying that particles position is localized at the center of the trap.

until a threshold voltage is reached where the particle does not seem to move any more. Fig. 15 shows optical pictures of such particles trapped in the donut nDEP cage.

<sup>1</sup>R. Pethig, *Biomicrofluidics* **4**, 022811 (2010).

<sup>2</sup>H. Morgan, D. Holmes, and N. G. Green, *IEEE Proc. Nanobiotechnol.* **150**(2), 76 (2003).

<sup>3</sup>D. Holmes, H. Morgan, and N. G. Green, *Biosens. Bioelectron.* **21**, 1621 (2006).

<sup>4</sup>H. Chu, I. Doh, and Y.-H. Cho, *Lab Chip* **9**, 686 (2008).

<sup>5</sup>C. Zhang, K. Khoshmanesh, F. Tovar-Lopez, A. Mitchell, W. Wlodarski, and K. Klantar-zadeh, *Microfluid. Nanofluid.* **7**, 633 (2009).

<sup>6</sup>H.-H. Cui, J. Voldman, X.-F. He, and K.-M. Lim, *Lab Chip* **9**, 2306 (2009).

<sup>7</sup>X.-B. Wang, J. Vykoukal, F. F. Becker, and P. R. C. Gascoyne, *Biophys. J.* **74**, 2689 (1998).

<sup>8</sup>H. Hu, Z. Y. Wang, R. F. Yue, and L. T. Liu, in *Proceedings of the 1st IEEE International Conference on Nano/Micro Engineered and Molecular Systems*, 21 January (2006), p. 18.

<sup>9</sup>D. Chen and H. Du, *Microfluid. Nanofluid.* **3**, 603 (2007).

<sup>10</sup>A. Docoslis and P. Alexandridis, *Electrophoresis* **23**, 2174 (2002).

<sup>11</sup>W. M. Arnold, *IEEE Trans. Dielectrics and Electrical Insulation* **15**, 144-151 (2008).

<sup>12</sup>M. Suzuki, T. Yasukawa, H. Shiku, and T. Matsue, *Langmuir* **23**, 4088 (2007).

<sup>13</sup>B. R. Burg, V. Bianco, J. Schneider, and D. Poulikakos, *J. Appl. Phys.* **107**, 124308 (2010).

<sup>14</sup>T. P. Hunt, D. Issadoreb, and R. M. Westervel, *Lab Chip* **8**, 81 (2008).

<sup>15</sup>T. Honegger, O. Lecarme, K. Berton, and D. Peyrade, *Microelectron. Eng.* **87**, 756 (2010).

<sup>16</sup>T. Honegger, O. Lecarme, K. Berton, and D. Peyrade, *J. Vac. Sci. Technol. B* **28**, C6114 (2010).

<sup>17</sup>H. Pohl, *J. Appl. Phys.* **22**, 869 (1951).

<sup>18</sup>V. Studer, A. Pepin, Y. Chen, and A. Ajdari, *Microelectron. Eng.* **62**, 915 (2002).

<sup>19</sup>A. Ramos, H. Morgan, N. G. Green, and A. Castellanos, *J. Phys. D: Appl. Phys.* **31**, 2338 (1998).

<sup>20</sup>A. Ramos, H. Morgan, N. G. Green, and A. Castellanos, *J. Electrostat.* **47**, 71 (1999).

<sup>21</sup>N. G. Green, A. Ramos, and H. Morgan, *J. Phys. D: Appl. Phys.* **33**, 632 (2000).

<sup>22</sup>A. Castellanos, A. Ramos, A. G. Iez, N. G. Green, and H. Morgan, *J. Phys. D: Appl. Phys.* **36**, 2584 (2003).



- <sup>23</sup>A. Rosenthal, a. B. M. Taffa, and J. Voldman, *Lab Chip* **6**, 508 (2006).
- <sup>24</sup>J. Oh, R. Hart, J. Capurro, and H. Noh, *Lab Chip* **9**, 62 (2009).
- <sup>25</sup>J. Voldman, R. A. Braff, M. Toner, M. L. Gray, and M. A. Schmidt, *Biophys. J.* **80**, 531 (2001).
- <sup>26</sup>A. Rosenthal and J. Voldman, *Biophys. J.* **88**, 2193 (2005).
- <sup>27</sup>T. Muller, G. Gradl, S. Howitz, S. Shirley, T. Schnelle, and G. Fuhr, *Biosens. Bioelectron.* **14**, 247 (1999).
- <sup>28</sup>T. Honegger, K. Berton, T. Pinedo-Rivera, and D. Peyrade, *Microelectron. Eng.* **86**, 1401 (2009).
- <sup>29</sup>F. S. O. Fritzsche, K. Rosenthal, A. Kampert, S. Howitz, C. Dusny, L. Blank, and A. Schmid, *Lab Chip* **13**, 397–408 (2012).
- <sup>30</sup>T. Honegger, M. A. Scott, M. F. Yanik, and J. Voldman, *Lab Chip* **13**, 589 (2013).
- <sup>31</sup>J. Suehiro and R. Pethig, *J. Phys. D: Appl. Phys.* **31**, 3298 (1998).
- <sup>32</sup>M. Li, S. Li, W. Cao, W. Li, W. Wen, and G. Alici, *Microfluidics and Nanofluidics* (Springer-Verlag, 2012), pp. 1–13.
- <sup>33</sup>M. Muratore, V. Srsen, M. Waterfall, A. Downes, and R. Pethig, *Biomicrofluidics* **6**, 034113 (2012).
- <sup>34</sup>M. J. Gordon and D. Peyrade, *Appl. Phys. Lett.* **89**, 053112 (2006).
- <sup>35</sup>C. Renaut, J. Dellinger, B. Cluzel, T. Honegger, D. Peyrade, E. Picard, F. de Fornel, and E. Hadji, *Appl. Phys. Lett.* **100**, 101103 (2012).
- <sup>36</sup>M. P. Hughes, H. Morgan, and M. F. Flynn, *J. Colloid Interface Sci.* **220**, 454 (1999).
- <sup>37</sup>N. G. Green and H. Morgan, *J. Phys. Chem. B* **103**, 41 (1999).
- <sup>38</sup>I. Ermolina and H. Morgan, *J. Colloid Interface Sci.* **285**, 419 (2005).
- <sup>39</sup>T. Honegger, K. Berton, E. Picard, and D. Peyrade, *Appl. Phys. Lett.* **98**, 181906 (2011).
- <sup>40</sup>T. Honegger and D. Peyrade, *Biomicrofluidics* **6**, 044115 (2012).
- <sup>41</sup>T. Honegger, S. Sarla, O. Lecarme, K. Berton, A. Nicolas, and D. Peyrade, *Microelectron. Eng.* **88**, 1852 (2011).
- <sup>42</sup>C. Chung, M. Waterfall, S. Pells, A. Menachery, S. Smith, and R. Pethig, *J. Electr. Bioimp.* **2**, 64 (2011).
- <sup>43</sup>N. Islam, M. Lian, and J. Wu, *Microfluid. Nanofluid.* **3**, 369 (2007).
- <sup>44</sup>P.-Y. Chiou, A. T. Ohta, A. Jamshidi, H.-Y. Hsu, and M. C. Wu, *J. Microelectromech. Syst.* **17**, 525 (2008).
- <sup>45</sup>R. Micheletto, H. Fukuda, and M. Ohtsu, *Langmuir* **11**, 3333 (1995).
- <sup>46</sup>T. Honegger, K. Berton, O. Lecarme, L. Latu-Romain, and D. Peyrade, *Micro Nanosyst.* **2**, 239 (2010).
- <sup>47</sup>C. M. Pedersen, Master thesis, Technical University of Denmark, 2006.
- <sup>48</sup>R. S. Thomas, H. Morgan, and N. G. Green, *Lab Chip* **9**, 1534 (2009).
- <sup>49</sup>T. Schnelle, T. Muller, and G. Fuhr, *J. Electrostat.* **50**, 17 (2000).
- <sup>50</sup>C. H. Kua, Y. C. Lam, I. Rodriguez, C. Yang, and K. Youcef-Toumi, *Anal. Chem.* **80**, 5454 (2008).
- <sup>51</sup>C. H. Kua, Y. C. Lam, I. Rodriguez, C. Yang, and K. Youcef-Toumi, *Anal. Chem.* **79**, 6975 (2007).
- <sup>52</sup>T. Honegger and D. Peyrade, *Lab Chip* **13**, 1538 (2013).
- <sup>53</sup>P. Tabeling, *Introduction a la microfluidique* (Belin, 2003).
- <sup>54</sup>N. Loucaides, A. Ramos, and G. Georghiou, *J. Electrostat.* **69**, 111 (2011).
- <sup>55</sup>C. Dalton and K. V. I. S. Kaler, *Sens. Actuators B* **123**, 628 (2007).
- <sup>56</sup>M. Dürr, J. Kentsch, T. Müller, T. Schnelle, and M. Stelzle, *Electrophoresis* **24**, 722 (2003).
- <sup>57</sup>I. F. Sbalzarini and P. Koumoutsakos, *J. Struct. Biol.* **151**, 182 (2005).
- <sup>58</sup>Y. J. Yuan, M. K. Andrews, and B. K. Marlow, *Appl. Phys. Lett.* **85**, 130 (2004).
- <sup>59</sup>B. M. Taff and J. Voldman, *Anal. Chem.* **77**, 7976 (2005).